Alternative splicing of a potato disease resistance gene maintains homeostasis between development and immunity, and functions as a novel process for pathogen surveillance

Biying Sun[1,2], Jie Huang[1,2], Chuyun Gao[1,2], Kangping Li[1], Fei Zhao[1], Liang Kong[1,2], Luyao Wang[1,5], Jiayong Shen[1], Yuanchao Wang[1,2], Dennis A. Halterman[3,4,*], Suomeng Dong[1,2,*]

[1]Department of Plant Pathology, Nanjing Agricultural University, Nanjing 210095, China.

[2]The Key Laboratory of Integrated Management of Crop Diseases and Pests (Ministry of Education), Nanjing Agricultural University, Nanjing 210095, China.

[3]Department of Plant Pathology, University of Wisconsin-Madison, Madison, Wisconsin, United States of America.

[4]U.S. Department of Agriculture-Agricultural Research Service, Vegetable Crops Research Unit, Madison, Wisconsin, United States of America

[5]Shenzhen Branch, Guangdong Laboratory of Lingnan Modern Agriculture, Genome Analysis Laboratory of the Ministry of Agriculture and Rural Affairs, Agricultural Genomics Institute at Shenzhen, Chinese Academy of Agricultural Sciences, Shenzhen, Guangdong, 518120, China.

*Address correspondence to: smdong@njau.edu.cn, dennis.halterman@usda.gov

Short title:

Resistance gene alternative splicing regulates development and immunity homeostasis

One-sentence summary:

Potato resistance gene *RB* balances plant growth and immunity through AS, while pathogen-secreted effector IPI-O1 mediates AS of *RB* by targeting the conserved splicing factor StCWC15, further increasing the *RB_CDS* expression level to activate immunity.

Abstract

Plants possess a robust and sophisticated innate immune system against pathogens. The intracellularly localized receptors with nucleotide-binding, leucine-rich repeat (NLR) motifs recognize pathogen-derived effector proteins to trigger the immune response. To balance plant growth with rapid pathogen detection, NLR expression is precisely controlled in multifaceted ways. The role of post-transcriptional processing of NLRs, including alternative splicing (AS) of introns, in response to infection is an important area of research that requires further study. Here we report that the potato NLR gene *RB* undergoes AS of its intron, resulting in two transcriptional isoforms, which coordinately regulate plant immunity and growth homeostasis. *RB* mainly exists as intron-retained isoform *RB_IR* encoding a truncated lost-function RB protein to maintain plant normal growth without pathogen infection. Upon late blight infection, the causal pathogen *Phytophthora infestans* induces intron splicing of *RB*, increasing the abundance of *RB_CDS*, which encodes a full-length, and active R protein. By deploying the *RB* splicing isoforms fused with *luciferase* reporter system, we identified IPI-O1 (also known as Avrblb1), the RB cognate effector, as a facilitator of *RB* AS. Importantly, IPI-O1 directly interacts with potato splicing factor StCWC15 to promote *RB* splicing for activation of *RB*-mediated resistance. Thus, our study reveals that StCWC15 serves as a surveillance facilitator sensing the pathogen-secreted effector maintaining the trade-off between *RB*-mediated plant immunity and growth, expanding our understanding of molecular plant-microbe interactions.

Keywords: potato late blight; resistance gene; RB; IPI-O1; CWC15

Introduction

Upon pathogen infection, plants have evolved two major mechanisms for recognition of pathogen effectors and elicitation of plant defense (Jones and Dangl, 2006). One utilizes plasma membrane-localized pattern-recognition receptors (PRRs) to perceive pathogen-associated molecular patterns (PAMPs), leading to PAMP-triggered immunity (PTI) (Couto and Zipfel, 2016). The other uses intracellular NLR immune receptors to detect cytoplasmic effectors introduced by the pathogen, thereby activating effector-triggered

immunity (ETI; Jones and Dangl, 2006; Dodds and Rathjen, 2010; Cui et al., 2015). During ETI, NLRs oligomerize to form “resistosome” structures (Wang et al., 2019; Ofir et al., 2021) and the response culminates in programmed cell death, known as the hypersensitive response (HR), to prevent pathogen spread. The enormous diversity of *NLR* genes in plants demonstrates their important role in plant immunity (Li et al., 2015; Van de Weyer et al., 2019).

Late blight, caused by oomycete *Phytophthora infestans*, is the most devastating disease in potato production (Haverkort et al., 2009; Kamoun et al., 2015; Sun et al., 2022). Deployment of host resistance (R) genes is a crucial strategy for controlling the disease and many potato cultivars have been bred to introduce resistance genes against *P. infestans* (*Rpi* genes) that originate from potato wild relatives (Kamoun and Smart, 2005; Karki et al., 2021). More than 70 *Rpi* genes have been identified and mapped in 32 *Solanum* species (Paluchowska et al., 2022). Among these *R* genes, *RB* was cloned from the wild diploid potato species *Solanum bulbocastanum*, and is known for its durable late blight resistance (Song et al., 2003; van der Vossen et al., 2003). Like most plant *R* genes, *RB* encodes an NLR protein. It recognizes *P. infestans* effector IPI-O1 (also known as Avrblb1) to activate immune responses (Vleeshouwers et al., 2008; Champouret et al., 2009). Previous research has demonstrated that IPI-O1 could be recognized by RB and hypothesized that IPI-O1 changes the conformation of RB to facilitate the formation a functional multimeric complex, thereby activating *RB*-mediated disease resistance (Chen et al., 2012; Zhao and Song, 2021).

Despite their usefulness in activating resistance, constitutive expression of *NLR* genes causes auto-immunity, leading to a negative effect on plant growth and development (Cheng et al., 2011; Deng et al., 2019; Cui et al., 2020). Therefore, the expression of *NLR* genes needs to be precisely regulated to maintain homeostasis between growth and immunity. The regulation mechanisms for the expression of NLRs are mainly via transcription regulation, RNA processing, post-translational modification and proteasome-mediated degradation (Li et al., 2015). Intron splicing is common in post-transcriptional RNA processing and is executed by a supramolecular ribonucleoprotein (RNP) complex known as the spliceosome (Reddy, 2007). Intron retention during RNA processing is a form of alternative splicing (AS) and can lead to changes in the translated protein. AS contributes to transcriptome and proteome

diversity in animals and plants and it has been shown to play an important role in regulating plant immunity (Reddy et al., 2013b; Wu et al., 2016; Bazin et al., 2020; Zhang et al., 2022). Several *NLR* genes have been demonstrated to undergo AS, suggesting that this may be an important mechanism for regulation of this important class of immunity-related genes (Dinesh-Kumar and Baker, 2000; Halterman et al., 2003; Halterman and Wise, 2006; Sanchez-Martin et al., 2021). The splicing regulation of NLR had been reported (Xu et al., 2012). However, the molecular mechanisms that control *NLR* gene AS and the significance of AS in maintaining plant growth and immunity homeostasis is incompletely understood.

In this work, we report that the potato resistance gene *RB* undergoes alternative splicing, resulting in generation of two transcripts. Removal of the intron results in intact RB protein that confers resistance to *P. infestans*, while intron retention results in a truncated RB protein that cannot protect against the pathogen. Upon late blight infection, *P. infestans* is able to modulate the AS of *RB*, increasing the abundance of *RB_CDS* to activate *RB*-mediated immunity. Interaction of *P. infestans* effector IPI-O1 with splicing factor CWC15 in the nucleus leads to an increase of *RB* intron splicing during infection. This process balances plant growth and defense and provides a unique molecular basis for NLR recognition of pathogen effectors.

Results

P. infestans promotes *RB* intron splicing

The *RB* gene contains a single 679nt intron beginning 428nt downstream of the translation start codon (Figure 1A). To investigate AS of the *RB* intron, we performed rapid amplification of cDNA ends (5' RACE) using RNA from non-inoculated *RB* transgenic potato cv. Katahdin expressing a single genomic copy of *RB* with its native promoter (SP951; Bradeen et al., 2009). Two transcriptional isoforms were identified that correspond to the transcripts with the intron spliced (*RB_CDS*) or retained (*RB-IR*) (Fig. 1A and Supplemental Fig. S1). We further examined AS of *RB* in SP951 and *RB* transgenic *Nicotiana benthamiana* by reverse transcription PCR (RT-PCR). We identified two transcripts corresponding to *RB_CDS* and *RB_IR* in plants with *RB*, but no transcripts in non-transgenic controls (Fig. 1B). Splicing of introns in pre-mRNA is directed by spliceosome targeting of particular sequences

at the intron/exon junctions called splice sites (Wan et al., 2020) and are commonly found with a conserved GT dinucleotide at the 5' splice site and a conserved AG dinucleotide at the 3' splice site (Sheth et al., 2006). We synonymously mutate the splice sites in *RB* from GT to GA (5') and from AG to CG (3') resulted in the inability of transiently expressed *RB_IVS* (IVS=intervening sequence) to undergo intron splicing in both potato and *N. benthamiana* (Fig. 1B). Among the two transcripts of *RB*, *RB_CDS* encodes the entire NLR protein, while *RB_IR* encodes a truncated protein containing only the CC domain, due to a premature termination codon (PTC) in the intron (Fig. 1C). Immunoblot analysis revealed that the translation products from both RB_CDS and RB_IR with Myc tags can be detected (Fig. 1D).

To investigate the dynamic change of *RB* splicing during pathogen infection, we inoculated *RB* transgenic potato SP951 with *P. infestans* isolate JH19 and measured the transcript levels of different isoforms of *RB* compared to levels following water (mock) inoculation. The results show that the relative expression intensity of the *RB_IR* isoform was reduced at 1 and 2 dpi, whereas the relative expression intensity of the *RB_CDS* isoform increased during the same timeframe (Fig. 2A). We also inoculated SP951 with zoospores of *Phytophthora capsici* isolate LT1534 and monitored the level of transcripts compared to mock. We found that *P. capsici* had no effect on the relative expression of either *RB* transcript (Fig. 2A). Quantitative RT-PCR data demonstrated that the splicing ratio (transcript level of the spliced isoform divided by the transcript level of the unspliced isoform) of *RB (RB_CDS/RB_IR)* significantly increased to 1.66 at 1 dpi and 2.78 at 2 dpi following JH19 inoculation, indicating an increase in *RB_CDS* expression and a decrease of *RB_IR* expression during *P. infestans* infection (Fig. 2B and Supplemental Fig. S2A). *RB* splicing ratios remained unchanged in *P. capsici* inoculated plants and mock treatment (Fig. 2B and Supplemental Fig. S2A). Following these experiments, we found the total gene expression of *RB* did not change significantly in either *P. infestans*-, *P. capsici*-, or mock-inoculated plants (Supplemental Fig. S2B). Together, these results indicate that the *RB* gene produces more *RB_CDS* transcript due to increased intron splicing following inoculation of *P. infestans*.

Intron splicing of *RB* is necessary for the activation of resistance and functions independent of ETI

To test whether intron splicing can impact the ability of *RB* to confer *P. infestans* resistance, we stably transformed wild-type *RB*, *RB_CDS*, *RB_IR*, and *RB_IVS* into potato cultivar Favorita. We found the multiple potato plants expressing the wild-type *RB* and *RB_CDS* exhibited clear resistance to *P. infestans*, while plants expressing *RB_IR* or *RB_IVS* showed severe disease symptoms (Fig. 3A). The results of detached leaf assays of the transgenic potatoes were consistent with the whole plant phenotypes (Fig. 3B). We also created *RB*, *RB_CDS*, *RB_IR*, and *RB_IVS* transgenic *N. benthamiana* for our assays, and found that *RB* and *RB_CDS* limited *P. infestans* lesion development and induced an HR following expression of the *RB*-corresponding effector IPI-O1, while *RB_IR* and *RB_IVS* did not (Supplemental Fig. S3).

The splicing process is executed by the spliceosome, which is conserved in eukaryotes and is dynamically composed of a ribonucleoprotein complex (Chen and Manley, 2009). We further tested whether AS of *RB* and immunity activation induced by *P. infestans* is affected following silencing of spliceosome core components. We silenced orthologs of *U1-70k* (Chen et al., 2020) and *SF3B1* (Finci et al., 2018) in *N. benthamiana* to test the effect on activation of resistance mediated by intron-containing NLR and intron-lacking NLRs. Following silencing of *U1-70k* and *SF3B1*, co-infiltration of the intron-containing *NLR* genes *RB* or *Rpi-blb2* with the corresponding effectors *IPI-O1* and *Avrblb2*, respectively, elicited a significantly weakened HR (Supplemental Fig. S4, A-C). However, co-infiltration of the intronless NLRs *RB_CDS* or *R3a* with the corresponding effectors *IPI-O1* and *Avr3a*, respectively, induced a strong HR following silencing of *U1-70k* and *SF3B1* (Supplemental Fig. S4, A-C). We also silenced the RNA-binding protein *GRP7*, which is reported to regulate RNA processing to affect the PTI response and specifically affect NLR protein Gpa2/Rx1 mediated immunity (Wang et al., 2020; Sukarta et al., 2022). *GRP7* silencing had no effect on suppression of the HR following co-infiltration of any tested NLRs with their corresponding effectors (Supplemental Fig. S4, A-C). We further silenced *U1-70k*, *SF3B1*, and *GRP7* in *RB* transgenic *N. benthamiana* to test their effect on *RB*-mediated resistance to *P. infestans*. The results show that silencing of *U1-70k* and *SFB1* rendered *RB* transgenic *N. benthamiana* susceptible to *P. infestans* compared to the EV control (Fig. 4, A and B). However, it was observed that the silencing of *GRP7* did not have a significant effect on *RB*-mediated

resistance (Fig. 4, A and B). Previously, we have observed that the *RB_CDS* transcript isoform was most prevalent following *P. infestans* infection. We therefore tested the effect of *U1-70k*, *SF3B1*, and *GRP7* on *RB* AS. The quantitative PCR results indicated that silencing of *U1-70k* and *SF3B1* both significantly suppressed *RB* splicing ratio up-regulation following *P. infestans* inoculation compared to the water-inoculated control (Fig. 4C and Supplemental Fig. S4D). Consistent with our previous results, silencing of *GRP7* did not affect the induction of *RB* splicing following infection (Fig. 4C and Supplemental Fig. S4D). To further validate the role of the intron splicing in *RB* function, we conducted a chemical splicing inhibitor assay. The splicing modulator Pladienolide B (Pla-B), interferes with splicing by targeting SF3B1 and inhibiting its proper recognition with the intron (Kotake et al., 2007; Cretu et al., 2018). We found that treatment with 30 μM Pla-B significantly reduced the incidence of HR following co-infiltration with *RB*/*IPI-O1*, but did not affect HR incidence following *RB_CDS*/*IPI-O1* co-infiltration (Fig. 4D). Furthermore, we examined splicing ratio changes of *RB* induced by *P. infestans* following Pla-B treatment. The transcript-expression analysis indicates 30μM Pla-B repressed the splicing ratio increase during infection (Fig. 4E and Supplemental Fig. S4E). These results suggest that *P. infestans* modulates *RB* pre-mRNA AS changes to initiate *RB* immune responses.

IPI-O1 mediates *RB* splicing during the infection process

To determine the specific protein secreted by *P. infestans* to regulate *RB* intron splicing, we designed an *RB* alternative splicing reporter system that can directly reflect the extent of *RB* intron splicing. The *RB* AS reporter system can detect the modulation of intron splicing without ETI activation. The reporter is made up of the AS region of *RB* genomic sequences (from 1 nt to 1987 nt) fused with the luciferase (*LUC*) reporter gene downstream of the intron splicing site. The *RB-LUC* reporter system is predicted to produce two transcripts (Fig. 5A): the first is *RB_IR-LUC*, which retains the intron, introduces a premature termination codon, and does not produce a LUC signal; the second is *RB_CDS-LUC*, in which the intron is spliced and translates a complete RB CC-NB protein and functional LUC protein. To further verify the intron splicing changes via the *RB* AS reporter system following *P. infestans* inoculation, we transiently expressed *RB-LUC* using agrobacterium in *N. benthamiana* and

inoculated with *P. infestans* JH19. Luciferase activity was measured at 1 dpi and demonstrated a significant increase of LUC activity produced by *RB-LUC* compared to the mock (water-inoculated), whereas the LUC activity of *RB_CDS-LUC* and *LUC* control constructs did not change following *P. infestans* inoculation (Supplemental Fig. S5). Taken together, we verified the modulation of *P. infestans* on promoting *RB* intron splicing by the *RB* AS reporter system, demonstrating the feasibility of this system. This supported using the *RB* AS reporter system to screen for *P. infestans* effectors that promote RB splicing. Indeed, we previously identified several splicing regulatory effectors (SRE) using another splicing reporter system (Huang et al., 2020). To determine whether these SRE proteins specifically modulate *RB* splicing, we co-expressed several SRE proteins with the *RB-LUC* reporter system in *N. benthamiana*. Screening results show that only IPI-O1 (SRE8) significantly induced *RB* intron splicing compared to the mock-infiltrated control (Fig 5B). Infiltration of SRE proteins with *RB_CDS-LUC*, which lacks the intron, did not affect LUC activity (Fig. 5, B and C). To further verify the relationship between SRE proteins regulating *RB* AS and activation of *RB* resistance, we overexpressed SRE proteins in *RB*-transgenic *N. benthamiana* leaves to observe *RB* splicing changes and HR elicitation. Consistent with screening results on the *RB* AS reporter system, overexpression of IPI-O1 induced *RB* intron splicing and elicitation of the HR, while overexpression of other SRE proteins had no effect on either response (Supplemental Fig. S6). Overall, these data suggest that IPI-O1, the corresponding effector of *RB*, promotes AS of the *RB* gene.

Nuclear localization of IPI-O1 is required for RB-induced immune response

IPI-O1 has been reported as a nuclear-localized effector protein (Wang et al., 2018), and we further predicted the presence of a nuclear localization signal (NLS) motif within the protein. Given that IPI-O1 can affect *RB* splicing and that it is localized to the nucleus, we tested whether subcellular localization of IPI-O1 is correlated with its ability to affect *RB* splicing and HR-elicitation activity. We generated an IPI-O1 mutant, IPI-O1^{nls}, in which a total of seven key NLS motif amino acids K (lysine) and R (arginine) were mutated to A (alanine), and monitored the subcellular localization of proteins by confocal microscopy (Fig. 6A). We found that IPI-O1^{nls} fails to accumulate in the nucleoplasm and nucleolus like

IPI-O1, and instead is localized primarily in the cytoplasm (Fig. 6, B-D). Next, we tested the ability of IPI-O1^{nls} to induce the HR. The results showed that IPI-O1 induced the HR in both *RB* and *RB_CDS* transgenic *N. benthamiana*, but not in *RB_IR* plants (Fig. 6E). The IPI-O1^{nls} mutant failed to induce the HR in *RB N. benthamiana*, but was still able to elicit the HR in *RB_CDS* transgenic *N. benthamiana* (Fig. 6E). We then examined IPI-O1 and IPI-O1^{nls} function on the modulation of *RB* intron splicing and found that the *RB_CDS*/*RB_IR* splicing ratio increased during overexpression of IPI-O1 but not IPI-O1^{nls} (Fig. 6F). Together, these data suggest that *RB* intron splicing and immunity activation requires nuclear localization of IPI-O1. Consistent with the splicing ratio analysis by RT-qPCR (Fig. 6F), the *RB-LUC* reporter system verified that IPI-O1, but not IPI-O1^{nls}, significantly promoted *RB* splicing (Fig. 6G). In conclusion, the nuclear localization of IPI-O1 has an effect on promoting *RB* intron splicing and immunity activation, but it has no impact on the function of the intron-spliced *RB_CDS*.

IPI-O1 interacts physically with splicing factor CWC15 in the nucleus

To identify the potential splicing regulators of *RB*, we performed an ULTImate (Hybrigenics) yeast-two hybrid (Y2H) screen to identify IPI-O1-interacting proteins within a *N. benthamiana* cDNA library. A total of 81.6 million interactions were analyzed and 254 clones were processed by sequencing of the prey inserts. Of these 254 clones, 28 contained an insert with homology to the *CWC15* gene from *N. tomentosiformis* (LOC104090615). CWC15 is a core component of the Nineteen complex within the spliceosome (Will and Lührmann, 2011). We identified two *CWC15*-related gene sequences in the double-monoploid potato DM-1-3: *Soltu.DM.10G000900.1* (*StCWC15a*) and *Soltu.DM.07G027590.1* (*StCWC15b*), which encoded 231 aa (amino acid) and 228 aa proteins respectively. StCWC15a and StCWC15b share 93% similarity at the amino acid levels (Supplemental Fig. S7A). Y2H assays also verified the interaction of full-length NbCWC15a and NbCWC15b with IPI-O1 (Fig. 7A). Analysis of CWC15 sequence variation in multiple wild and cultivated potatoes determined that CWC15 is well conserved but polymorphisms are detected (Supplemental Fig. S7B).

To further explore the interaction between IPI-O1 and mutant IPI-O1^{nls} with CWC15a/b

in potato, we performed co-immunoprecipitation *in planta*. The results showed that both StCWC15a and StCWC15b interacted with IPI-O1, but the nuclear localization mutant IPI-O1^{nls} did not interact with either protein (Fig. 7B). No interaction was observed between StCWC15 proteins and *P. infestans* effector Pi04314, another RxLR effector that interacts with three host protein phosphatase 1 catalytic isoforms, causing their re-localization from the nucleolus to the nucleoplasm (Boevink et al., 2016). The interactions were verified *in vitro* by GST-pull down and Y2H, and were consistent with the co-IP assay (Fig. 7, C and D). These data demonstrated that interaction between IPI-O1 and StCWC15 proteins was abolished when the nuclear localization signal of IPI-O1 was mutated, indicating that nuclear localization is important for the interaction. We also performed bimolecular fluorescence complementation (BiFC) to investigate the subcellular localization of interaction between IPI-O1 and StCWC15. The results demonstrated that IPI-O1 interacted with StCWC15 proteins in nuclear speckles and the nucleolus (Supplemental Fig. S8). We did not observe fluorescence when testing the interaction between StCWC15 proteins and the IPI-O1^{nls} or Pi04314 (Supplemental Fig. S8). Both the nucleolus and nuclear speckles are cellular structures highly correlated with RNA splicing (Liao and Regev, 2021). While expression of fusion proteins of StCWC15a and StCWC15b with the red fluorescence protein (RFP) demonstrated that StCWC15a primarily localized to the nucleoplasm (91%), the protein was occasionally found in the nucleolus (5%) and nuclear speckles (4%). StCWC15b was distributed similarly and was localized in the nucleoplasm (90%), nucleolus (5%) and nuclear speckles (5%) (Supplemental Fig. S9). To detect StCWC15 subcellular localization changes that may occur in the presence of the IPI-O1 effector, we co-expressed StCWC15a/b-RFP fusion proteins with GFP-IPI-O1 in *N. benthamiana*, with GFP-IPI-O1^{nls} and GFP protein alone as controls. The results showed that StCWC15a protein was re-localized into speckles (63%) or the nucleolus (26%), and that StCWC15b protein was re-localized into speckles (60%) or the nucleolus (25%) when co-expressed with IPI-O1, but not with IPI-O1^{nls} or GFP (Fig. 7E). To further investigate the re-localization of CWC15 during *P. infestans* infection, *N. benthamiana* expressing GFP–CWC15a/b was inoculated with zoospores of transgenic *P. infestans* isolate 88069 expressing the fluorescent protein RFP. The number of cells with speckle-localized CWC15 near the infected hyphae increased more than in cellsdistant from

the infected hyphae (Supplemental Fig. S10). *P. infestans* infection had no effect on nuclear localization of the GFP control (Supplemental Fig. S10). These results suggest that IPI-O1 interacts with StCWC15 proteins in the nucleus and induces their re-localization from the nucleoplasm into speckles and the nucleolus.

Silencing StCWC15 disrupts *RB*-mediated immunity

To determine the effect of CWC15 on *RB*-mediated immunity, we transiently silenced CWC15, transcription-related factors *PPS7*, (Katou et al., 2005), and splicing-related genrs *SR30*, and *RS2Z32* (Reddy, 2004) in *RB* transgenic *N. benthamiana* followed by transient expression of IPI-O1. Infiltrated areas were assayed for HR elicitation. We found that silencing of *CWC15* resulted in a reduced incidence of HR compared to the EV control, while *PPS7*, *SR30*, or *RS2Z32* silencing had no effect on RB recognition of IPI-O1 (Supplemental Fig. S11A). *SGT1* silencing, known to be required for *RB* function (Bhaskar et al., 2008), also reduced HR incidence compared to the EV control (Supplemental Fig. S11A). The effect of CWC15 on *R* gene function appeared to be specific for *RB*, as silencing of *CWC15* had no effect on the elicitation of HR following co-infiltration of *R1*, *Rpiblb2*, or *R3a* with their corresponding effectors, or following infiltration of elicitor *INF* (Supplemental Fig. S11B). Based on the transient screening results, we further verified the function of *CWC15* by virus-induced gene silencing (VIGS). The TRV-*NbCWC15* silenced plant exhibited small and short morphology compared to wildtype (Supplemental Fig. S12, A and B). Similar to the transiently silenced results, TRV-*NbCWC15* silenced plants were disturbed for the recognition of IPI-O1 by *RB* (Supplemental Fig. S12, C-E). Together, this indicated CWC15 as an interactor of IPI-O1 involved in *RB* activation. To verify the function of potato *CWC15* in *RB*-mediated immunity, we stably silenced *StCWC15* by introducing a hairpin-silencing construct in *RB*-transgenic potato by transformation. We obtained three independent transgenic lines in which *StCWC15* transcription was reduced and a susceptible phenotype was exhibited following inoculation with *P. infestans* when compared to the *RB* transgenic parent potato (Fig. 8, A-D). CWC15 has been reported to regulate alternative splicing in Arabidopsis (Slane et al., 2020). Therefore, we hypothesized that StCWC15 would play a role in *P. infestans*-induced AS of *RB*. To test this, we detected *RB* transcript levels in the

highest silencing efficiency line *RB-StCWC15* RNAi#2 following inoculation with *P. infestans* isolate JH19. We found that the *RB_CDS/RB_IR* splicing ratio remained constant in the *StCWC15* knockdown plant, while the ratio increased in the *RB* transgenic control plant (Fig. 8E). These data demonstrate that splicing factor CWC15 is involved in regulating *RB* splicing changes during *P. infestans* infection, thus affecting *RB*-mediated immunity in potato.

We further silenced *CWC15* using VIGS in *RB*, *RB_CDS* and *Rpi-blb2* transgenic *N. benthamiana*. We found that the silencing of *CWC15* significantly impaired IPI-O1 induced HR and resistance to *P. infestans* in the *RB* line. Silencing had no effect on the resistance of *RB_CDS* and *Rpi-blb2* transgenic lines, nor on the HR induced by Avr3a/R3a or INF1 (Fig. 8F and Supplemental Fig. S13) This data indicates that CWC15 specifically targets splicing of *RB* and does not affect the function of *RB* once the intron is removed. To validate the role of CWC15 in *RB*-mediated resistance, we complemented *StCWC15* in the TRV-*NbCWC15* silenced *RB* transgenic *N. benthamiana* using silencing-resistant *CWC15* synthetic constructs. These synthetic genes were constructed with shuffled synonymous codons and encode full-length StCWC15a/b (Supplemental Fig. S14A). The results showed that expression of StCWC15a^{syn} and StCWC15b^{syn} rescued the impaired HR and *RB* resistance in TRV silenced-*CWC15* transgenic plants (Fig. 8G and Supplemental Fig. S14B). Immunoblot analysis revealed that expression of StCWC15a^{syn} and StCWC15b^{syn} recovered the expression of CWC15 in silenced *N. benthamiana* (Supplemental Fig. S14, C and D). Collectively, our results indicate that IPI-O1 modulates splicing factor CWC15 to mediate the AS of *RB* and increase the expression level of resistant transcript *RB_CDS*, leading to activation of *RB*-mediated immunity.

Regulation of *RB* intron splicing is critical for balancing plant growth and immunity

Our previous results indicated that the intron within *RB* is primarily not spliced in the absence of pathogen infection, leading to a truncated protein that cannot induce immune responses. The presence of pathogen effector IPI-O1 in the nucleus leads to increased intron splicing and, presumably, increased translation of a full-length RB protein. This regulation suggests that the plant maintains *RB* in a non-spliced state during normal growth perhaps to

avoid auto-immunity responses that could impact growth and development. To test this, we generated *RB*, *RB_CDS*, and *RB_IR* transgenic lines in potato cultivar Favorita and assessed their growth characteristics. All three of these genes were driven by a 35S constitutive promoter. In the seedling stage, *RB_CDS* transgenic lines exhibited shorter stem height and root length than non-transformed Favorita, while *RB* and *RB_IR* transgenic lines were not significantly different (Fig. 9, A and B). We also found that *RB_CDS* transgenic potatoes displayed slower growth and dwarf phenotypes compared to the wild-type *RB* transgenic potatoes when grown in pots (Supplemental Fig. S15). We further assessed tuber production and found there was no significant difference of the total number of tubers per plant between any of the transgenic lines and non-transformed Favorita. However, the average yield per plant and the average individual tuber mass was significantly reduced in plants expressing *RB_CDS* compared with Favorita, while these traits in *RB* and *RB_IR* transgenic potatoes were not significantly altered (Fig. 9, C and D). Research has found that accumulation of salicylic acid (SA) in response to biotic stress will affect the growth of plants (Ning et al., 2017; Gao et al., 2021a; Gao et al., 2021b). We compared SA concentrations in *RB* and *RB_CDS* transgenic potatoes with non-transformed wildtype potatoes and found that SA accumulation in the *RB_CDS* transgenic line was higher than in wildtype and *RB* transgenic potatoes (Fig. 9E). The *SARD1* gene is a key regulator for SA synthesis and plant immunity (Zhang et al., 2010). We tested the expression of *SARD1* in transgenic potatoes by RT-qPCR and found it was up-regulated in *RB_CDS* transgenic potatoes compared to wildtype and *RB* transgenic potatoes (Fig. 9F). Transcription of the SA-regulated defense gene *PR1* was also up-regulated in *RB_CDS* transgenic potatoes compared to the wildtype and *RB* transgenic potatoes (Fig. 9G). These results indicate that the sustained expression of *RB_CDS* in the non-infected state leads to continuous activation of SA-mediated defense responses, which likely affects growth and tuber production.

Discussion

Our work has revealed a new model of regulation of plant immunity responses: a pathogen effector (IPI-O1) targets a component of the spliceosome (CWC15) to modulate intron splicing of a plant *NLR* gene (*RB*). This results in increased production of the

full-length NLR protein that can further activate immunity in the presence of the same effector. This study implicates the spliceosome as a sensor to surveil pathogen effector activity, and activate plant immunity through proper splicing of an *NLR*. In this model, the plant utilizes alternative intron splicing to regulate expression of the *NLR* to limit inappropriate stress-induced responses during normal growth (Fig. 10). Earlier studies indicate a direct interaction between IPI-O1 and RB (Chen et al., 2012), and that IPI-O1 and RB should be localized to the cytoplasm to induce the HR (Zhao and Song, 2021). Further evidence indicates that IPI-O1 also accumulates in the nucleus (Wang et al., 2018). Together with the data presented here, we propose that IPI-O1 should be present in both the cytoplasm and the nucleus in order to fully activate immunity in the presence of *RB*.

Pathogens and plants are eternally entrenched in molecular warfare utilizing an arsenal of microbial effector proteins that manipulate the host to cause disease, and an equally diverse set of host protein receptors that recognize the presence of pathogen effectors to activate immune responses. Given the complexity of possible interactions between host and pathogen molecules, it is no surprise that multiple mechanisms exist to mediate effector recognition and activate resistance. Classical activation models of NLR proteins and effectors include direct recognition, indirect recognition, integrated decoy, and activation traps (Duxbury et al., 2021). The simplest mechanism is direct interaction between NLR proteins and their corresponding effector, leading to changes in protein structure or location that results in resistance activation. An example of this is the flax (*Linum usitatissimum*) resistance proteins L5/L6/L7 that physically interact with effector AvrL567 of flax rust (*Melampsora lini*) to confer resistance (Dodds et al., 2006). The indirect recognition mechanisms are divided into the guardee and the decoy models. In the guardee model, the effectors target a defense-related protein, either through direct binding or protein modification, that is monitored by an NLR protein. When changes in the guarded protein are recognized, this leads to activation of the NLR protein and elicitation of immune responses (Dangl and Jones, 2001). As an example, the Arabidopsis NLR protein RPS2 guards protein RIN4 that is targeted by the pathogen-secreted effector AvrRpt2 (Axtell and Staskawicz, 2003). The decoy model is derived from the guardee model, but decoy proteins have no function in host defense or susceptibility in the absence of the NLR protein (van der Hoorn

and Kamoun, 2008; Zhou and Chai, 2008). The classical decoy protein in plants is PBL2, which is uridylylated by AvrAC, leading to recognition by the NLR protein ZAR1 (Wang et al., 2015). An integrated decoy is an extension of the decoy model where the effector target is fused directly with the NLR protein, such as the WRKY domain in RRS1 or the HMA domain in RGA5 (Cesari et al., 2014; Maqbool et al., 2015; Sarris et al., 2015). Our results demonstrate an additional mechanism of effector recognition in plants. IPI-O1 is one of multiple *P. infestans* effectors capable of reprogramming genome-wide alternative intron splicing of the host (Huang et al., 2020). The CWC15 protein, a component of the spliceosome, is translocated to the nucleolus in the presence of IPI-O1, leading to splicing of the intron within the *RB* gene. *RB* intron splicing is necessary for the expression of a full-length protein that can activate immunity. The outcome of this model is similar to TAL effector activation traps that result in increased transcription of multiple executor *R* genes (Bogdanove et al., 2010). However, in the case of IPI-O1, *RB* gene expression is likely regulated at the co-transcriptional or post-transcriptional level, and not by transcription activation through promoter binding as it is with TAL effectors.

Alternative splicing provides a major source of transcriptome and proteome diversity. In plants, it is estimated that between 42% and 61% of all gene transcripts are alternatively spliced (Filichkin et al., 2010; Lu et al., 2010b; Marquez et al., 2012; Reddy et al., 2013a; Klepikova et al., 2016). AS can increase the protein complexity derived from a single gene and can result in proteins that differ in subcellular localization, stability, or post-translational modifications. AS can also play a role in gene regulation at the RNA level (Jia et al., 2020) and, more specifically, in regulating plant immunity (Reddy, 2007; Huang et al., 2017; Reddy et al., 2020). Several NLR genes undergo AS in the coding sequence or untranslated regions (UTRs; Yang et al., 2014; Lai and Eulgem, 2018). Our data indicate that the *RB* gene produces two different transcripts that encode either a full-length NLR protein that can confer resistance to *P. infestans*, or a truncated protein with only the CC and partial NB domains. Premature termination codon (PTC)-containing transcripts that arise as a result of AS are often subjected to a nonsense-mediated mRNA decay (NMD) process that is intended to prevent their translation (Brogna and Wen, 2009). An analysis of transcripts produced during bacterial infection in Arabidopsis showed that the majority of CC (coiled coil)-NLR (65.1%)

and TIR (Toll-like, Interleukin 1)-NLR (81.2%) transcripts exhibit evidence of NMD (Jung et al., 2020). However, transcripts containing PTCs can be used to express the truncated protein or have functional relevance. A truncated NLR protein RBA1 that contains only the TIR domain can still recognize effector HopBA1 and induce cell death (Nishamura et al., 2017). The TIR-NBS truncated protein TN2 associates with and may stabilize calcium-dependent protein kinase5 to regulate defense responses (Liu et al., 2017; Nishimura et al., 2017). Our results indicate that the *RB* gene transcripts that retain the intron are still detectable by RT-PCR and the truncated RB_IR protein is detectable in plants (Fig. 1D), suggesting that the short transcripts are not immediately degraded through NMD. *RB_IR* is predicted to encode a truncated protein of 169 aa and we found that plants transformed with the *RB_IR* construct produced the truncated protein as expected, but did not confer resistance to the pathogen. We hypothesize that this transcript may have other functions for the plant. According to the sequence, this truncated protein still encodes the CC domain of RB. Previous evidence indicates that the CC domain of RB can self-oligomerize (Chen et al., 2012). It remains to be tested whether the truncated CC domain competes with the CC domain from full-length RB to form an inactive oligomerized resistosome during normal growth in order to avoid autoactivation due to RB self-oligomerization.

In addition to directly affecting the expression of *NLR* genes, AS plays a more global role in regulating plant disease resistance responses. Arabidopsis *snc1* mutants constitutively activate defense responses and have increased resistance to pathogens (Zhang and Li, 2005). A screen for suppressors of *snc1* revealed two *MOS* (modifier of *snc1*) genes, *MOS4* and *MOS14*, that are involved in mRNA splicing (Palma et al., 2007; Xu et al., 2011). MOS4 directly interacts with AtCDC15, a Myb transcription factor, which has significant homology to a component of the spliceosome Nineteen complex, and is essential for NPR4-independent disease resistance signaling (Palma et al., 2007). The MOS14 protein is similar to transportin-SR, which is necessary for nuclear import of serine-arginine (SR) rich proteins (Xu et al., 2011). The SR family of proteins are important in various aspects of RNA splicing (Reddy, 2004; Barta et al., 2008; Long and Caceres, 2008). The *mutation of mos14-1* in Arabidopsis affects splicing of *NLR* gene *SNC1* and *RPS4* and compromises RPS4-dependent immunity and basal resistance to *Pseudomonas syringae* DC3000 (Xu et al., 2011). In

Arabidopsis, *P. syringae* introduces small RNAs that silence *SWP73A*, a chromatin-remodeling gene that regulates expression of several *NLRs* through promoter binding and alternative splicing (Huang et al., 2021). *CDC5* has been reported to regulate alternative splicing of *RPS4*, which is important for RPS4 activity (Palma et al., 2007; Zhang and Gassmann, 2007). Although the IPI-O1 effector interacts with CWC15 to regulate the splicing of the *RB* gene, it seems unlikely that *RB* is its specific target. More likely, an IPI-O1/CWC15 complex affects AS at a global level. This is supported by previous data showing that IPI-O1 can regulate AS of immunity-related gene *RLPK* (Huang et al., 2020). The impact of this effector on regulation of plant defense responses will be a focus of future research.

For plants, homeostasis between growth and defense is vital for survival and reproduction in nature (He et al., 2022). Research on the role of *NLR* expression in regulating growth versus defense trade-offs in plants has been reported previously (Li et al., 2012; Tsuchiya and Eulgem, 2013; Cui et al., 2020; Huang et al., 2021). NLR proteins are the intracellular immune receptors and activators in plants. The transition between autoinhibited and activated states of NLRs is fine-tuned by intra- and inter-molecular interactions. Over-accumulation of R proteins could lead to autoimmunity (Dinh et al., 2022), whereas insufficient NLR expression could lead to pathogen susceptibility. We found that the intron within the coding sequence of *RB* is alternatively spliced and, under normal growth conditions, transcripts are maintained with the intron retained, leading to a truncated protein. Presumably, this is a strategy to reduce elicitation of immune responses in the absence of an invading pathogen by regulating expression of the full-length RB protein in the plant. This is supported by our results that overexpression of an *RB* gene with the intron removed leads to constitutive expression of defense-related genes, smaller plants, and lowered tuber yield. Following *P. infestans* inoculation to introduce the effector IPI-O1, *RB* produces more intron spliced *RB_CDS*, which encodes a full-length NLR protein to provide resistance.

Materials and methods

RT-qPCR analysis of *RB* splicing ratio and gene expression

Total RNA was extracted using E.Z.N.A.® Plant RNA Kit (R6827-01, OMEGA)

following the manufacturer's instructions and treated with RNase-Free DNase (M6101, Promega) to remove genomic DNA contamination. Approximately 700 ng RNA was used for reverse transcription with HiScript III 1st Strand cDNA Synthesis Kit (R312-01, Vazyme). RT-qPCR was performed with 2μL of 3-fold-diluted cDNA in a total reaction volume of 20μL in technical duplicates using ChamQ Universal SYBR qPCR Master Mix (Q711-02, Vayzme Biotech) with an ABI 7500 Fast Real-time PCR system according to the manufacturer's instructions. PCR conditions were as follows: 95°C for the 30s, followed by 40 cycles of 95°C for 5 s, 60°C for 34 s, and then 95°C for 15 s, 60°C for 1 min, 95°C for 30 s, 60□ for 15s for the melt curve. Relative transcript amount differences were calculated using the $2^{-\Delta\Delta CT}$ method in ABI 7500 System Sequence Detection Software. Three biological replicates were performed and the results showed similar trends.

Gene silencing and complementation in *N. benthamiana*

Virus-induced gene silencing (VIGS) was performed in *N. benthamiana* as previously described (Stam et al., 1997). For VIGS target design, the specific DNA fragments with 300 base pairs (bp) from GFP, *NbCWC15* (Niben101Scf04847g02012.1/Ni-ben101Scf00693g01009.1) predicted by VIGS tool (https://vigs.solgenomics.net/) were cloned into Tobacco Rattle Virus (TRV) construct. The sequences of the targets are listed in Supplemental Data Set S1. The constructs were introduced into *A. tumefaciens* GV3101 by electroporation. Suspensions of *A. tumefaciens* strain GV3101 harboring TRV1 and TRV2 constructs were mixed in a 1:1 ratio in infiltration buffer (10 mM MES, 10 mM $MgCl_2$ pH 5.6, and 150 uM acetosyringone) to a final OD_{600} of 0.4, and then left at room temperature for 2h. TRV2-EV was used as a negative control. Two-week-old *N. benthamiana* plants were infiltrated with *A. tumefaciens* for VIGS assays, and their upper leaves were used 2-3 weeks later. The silencing efficiency was confirmed by RT-qPCR. For the complementation assays, the shuffled synonymous synthetic *StCWC15* sequences were generated by Sangon Biotech and cloned into expression constructs pK7WGF2 with a C-terminal GFP tag. Synthetic proteins were detected by western blot.

The 300-bp fragment of *NbPPS7a/b*

(*Niben101Scf07798g01001.1*/*Niben101Scf01573g01003.1*), *NbSR30* (*Niben101Scf05298g04002.1*), *NbRS2Z32* (*Niben101Scf07227g00011.1*), *NbSGT1* (*Niben101Scf03241g00015.1*), *NbU1-70ka/b* (*NbS00011208g0006.1*/ *NbS00015731g0004.1*), *NbSF3b1a/b* (Niben101Scf06716g01016.1/ Niben101Scf06128g00004.1), *NbGRP7* (Niben101Scf00215g03004.1) were cloned and ligated into pK7GWIWG2D(II) to generate a hairpin silencing construct. The sequences of the targets are listed in Supplemental Data Set S1. The pK7GWIWG2D(II) empty vector was used as a control. Six- to seven-week *N. benthamiana* leaves were infiltrated with GV3101 *A. tumefaciens* strains containing either the silencing construct or empty vector control diluted to an OD_{600}=0.5.

Growth of plant material and microbial strains

Solanum tuberosum cv. Favorita and transgenic plants were grown on Murashige and Skoog (MS) medium in a growth chamber under 16 h light/8 h dark conditions at a constant temperature of 24 °C and light intensity of 100 μmol m^{-2} s^{-1}. Plants in soil were growth with 12 h light/12 h dark conditions at a constant temperature of 22°C and light intensity of 153 μmol m^{-2} s^{-1}.

N. benthamiana plants were grown and maintained in the greenhouse with 16 h light at 25°C and 8 h dark at 20°C throughout the experiments. *P. infestans* strains JH19, and 88069^{td}, expressing the red fluorescent marker tandem dimer RFP (tdTomato) (Dagdas et al., 2016) were grown on rye sucrose agar (RSA) at 18°C. *P. capsici* strain LT1534 was grown on V8 medium at 25□. *Escherichia coli* strains DH5α, JM109, and BL21 and *A. tumefaciens* strain GV3101 were grown on Luria-Bertani (LB) medium at 37 °C and 30 °C, respectively.

Plasmid construction

All primers and plasmids used for cloning and experiments are listed in Supplemental Data Set S2. All the templates used for PCR amplification come from genomic DNA (gDNA) or complementary DNA (cDNA) of *P. infestans* (strain T30-4), *N. benthamiana*, and *Solanum tuberosum* cv. Favorita using 2 × Phanta Max Master Mix (P515-01, Vazyme Biotech). FastPure Plasmid Mini Kit, FastPure Gel DNA Extraction Mini Kit and ClonExpress Ultra One Step Cloning Kit (Cat No. DC201-01, DC301-01 and C115-01) were used for nucleic

acid purification, digestion, and ligation.

Co-immunoprecipitation assays and GST pull-down

The *IPI-O1* gene without the signal peptide was inserted into pK7WGF2 with N-terminal RFP tag using ClonExpress Ultra One Step Cloning Kit (C115-01, Vazyme Biotech), and *StCWC15a/b* were inserted into pK7WGF2 with C-terminal GFP for expression in *N. benthamiana*. Leaves of 6-week-old *N. benthamiana* plants were co-infiltrated with RFP-tagged *IPI-O1*, GFP-tagged *StCWC15a/b*, and the P19 silencing suppressor. Two days after agro-infiltration, the leaves were frozen in liquid nitrogen and ground to powder using a mortar and pestle. Proteins were extracted with extraction buffer (10% [vol/vol] glycerol, 25mM Tris pH=7.5, 1mM EDTA, 150mM NaCl, 2% [wt/vol] PVPP, 10mM DTT, 1×Protease Inhibitor Cocktail (Sigma-Aldrich), 0.1% Tween 20). The samples were centrifuged at 4°C for 20 min at 12,000 × g, and the supernatant was transferred to a new tube. For GFP-IP, 1 mL of supernatant was incubated at 4°C for 2 h with GFP-Trap_A beads (Chromotek, Planegg-Martinsried, Germany). The beads were collected by centrifugation at 800 × g and washed four times in 1 mL washing buffer (25 mM Tris pH=7.5, 150 mM NaCl and 1mM EDTA, 10% [vol/vol] glycerol, 0.1% Tween 20). The beads were boiled for 10 min at 95°C. SDS-PAGE was performed with the supernatant, and co-IP of StCWC15a/b with IPI-O1 was detected using anti-GFP or anti-RFP (Chromotek, Planegg-Martinsried, Germany).

For *in vitro* GST pull-down assays, GST-StCWC15a/b and His-IPI-O1 were expressed in *E. coli* strain BL21. Co-precipitation of StCWC15a/b with IPI-O1 was examined by protein blotting before (input) and after affinity purification (pull-down) using glutathione agarose beads (GE Healthcare). Interactions were detected using anti-GST and anti-His (Abmart).

***P. infestans* and *P. capsici* infection assays**

P. infestans strains were grown on RSA medium plate at 18°C for 14 d. The sporangia were scraped into cold, distilled water and incubated at 4°C for 1-2 h until zoospore release. The zoospore suspension was adjusted to 100 zoospores/μL before inoculation. Ten microliter drops of *P. infestans* zoospores were placed on the abaxial side of detached leaves. The inoculated leaves were kept at 18°C for 4-7 days. The whole potato infection assays used a zoospore suspension sprayed on the plant followed by incubation in a controlled

environment chamber at 20°C for 6 days. The infected *N. benthamiana* leaves were stained with trypan blue. Leaves were soaked in trypan blue solution (10 mL 85% lactic acid aqueous, 10 mL water-saturated phenol, 10 mL 98% glycerol, 10 mL distilled water, 15 mg trypan blue) overnight. Stained leaves were then transferred into ethanol and incubated at 37°C for 24 h before observation. *P. capsici* strains were grown on V8 medium plate at 25℃ for 3 d. Then cut 10 pieces of mycelium with a size of about 2 mm^2 and culture them in V8 liquid medium for 4 days. Discard the culture medium, wash the mycelium with distilled water three times, add distilled water just enough to cover the mycelium, and incubate at 25℃ for 12 hours until *P. capsici* produces mature sporangia, placed at 4°C for 20 minutes to stimulate zoospores release.

Agroinfiltrations

Construct plasmids were transformed into *A. tumefaciens* strain GV3101 and grown overnight in Luria-Bertani (LB) culture medium with the antibiotics kanamycin and rifampicin at 30°C. Bacteria were harvested by centrifugation at 5000g for 4 min and then resuspended and diluted in an agroinfiltration buffer (10 mM $MgCl_2$, 150 mM acetosyringone, 10 mM MES) to an optical density of OD_{600} = 0.01–1.0 depending on the experiments. After 2-4 h of incubation at room temperature, they were infiltrated with a needleless syringe into the abaxial side of leaves from 4–5-week-old *N. benthamiana* plants. For the co-expression of multiple constructs, suspensions carrying each construct were thoroughly mixed before infiltration.

Confocal microscopy and bimolecular fluorescence complementation (BiFC) assays

Confocal microscopy was performed on N. benthamiana leaf patches post infiltration by LSM 980 laser-scanning microscope with 20×/0.8 or 60×/0.95 objective lens (ZEISS LSM 980 with Airyscan2). Parameters that are used for fluorescence detection are GFP/YFP, (excitation 488 nm, emission 505–540 nm), RFP (excitation 514 nm, emission 518–582 nm), DAPI (excitation 405 nm, emission 430–480 nm). Leaves were stained with 2 μg/mL of 4', 6-diamidino-2-phenylindole (DAPI) for 5 min to indicate nuclei. ZEISS ZEN Microscope Software was used to process the images.

pGTQL1221YC and pGTQL1211YN (nYFP/cYFP) vectors were used for Bimolecular

fluorescence complementation (BiFC) assays (Lu et al., 2010a). Coding regions of *IPI-O1* and *IPI-O1*^{nls} without a signal peptide and *StCWC15a/b* were amplified with primers containing attB tails and BP-cloned into pDONR207 (Invitrogen). To generate BiFC constructs, constructs were integrated into destination vectors pGTQL1221YC or pGTQL1211YN by LR recombination using Gateway LR clonase II (Invitrogen). The constructs were transformed into *A. tumefaciens* strain GV3101. Two days after agroinfiltration, the Zeiss 980 laser scanning confocal microscope was used for YFP fluorescence detection.

Transformation of potato and RNAi in potato

For generating transgenic potato, the entire *RB* gene sequence (3592 bp), *RB_CDS* transcript (2913 bp), *RB_IR* transcript (507 bp) were cloned into pBinGFP2 binary vector containing the *CaMV35S* promoter. The constructs were transformed into the *A. tumefaciens* strain GV3101. To generate stable transgenic potato plants, stems were used for transformation. Stem segments of *Solanum tuberosum* cv. Favorita were incubated in MS-medium (Murashige and Skoog, 1962). Agrobacterium containing each plasmid was grown and diluted to a cell concentration of OD_{600}=0.5. Stem segments were added and incubated in the dark for 45 mins. After co-incubation, stem segments were transferred to MS solid medium supplemented with 2.5 mg/L zeantinribose, 0.2 mg/L NAA, 0.02 mg/L GA_3 for 48 hours. After that, stems were washed with 300mg/L Timentin and transferred to MS solid medium supplemented with 2.5 mg/L zeantinribose, 0.2 mg/L NAA, 0.02 mg/L GA_3 and 200 mg/L Timentin for 2 weeks. For callus induction, stems segments were kept on MS solid medium with 2 mg/L zeantinribose, 0.02 mg/L NAA, 0.02 mg/L GA_3, 300 mg/L Timentin and 50 mg/L kanamycin. Every 14 days, stem segments or developing calli were placed onto new medium. After bud initiation formation (following 4-5 transfers), shoots were cut off from the callus and transferred to MS-medium containing 300 mg/L Timentin and 50 mg/L kanamycin.

For hairpin RNA interference (RNAi), the chalcone synthase (CHSA) intron was amplified from plasmid pFGC5941 The PCR-amplified 3′StCWC15 cDNA fragments overlapped the 5′ and 3′ end of the CHSA intron from two directions. The overlapped

fragment was inserted in the p1300 vector and transformed into *A. tumefaciens* strain GV3101 before potato transformation. Transformation is the same as potato stable overexpression transformation. *StCWC15s* silencing transgenic lines were confirmed by RT-qPCR in buds using the primers indicated in Supplemental Data Set S2.

5' RACE

Rapid amplification of cDNA ends (5' RACE) was used to determine the transcripts of the *RB* gene using the SMARTer RACE cDNA Amplification Kit (Clontech) according to the protocol. For synthesis of first-strand cDNA, we designed the *RB* specific primer (Supplemental Data Set S2). Next, we used 10 μM *RB* specific primer and the provided UPM primer in the kit for RACE PCR. Amplification was performed using a touchdown PCR protocol with five cycles of 94°C for 30 s, 72°C for 4 min, then five cycles of 94°C for 30 s, 70°C for 30s, 72°C for 4 min, final 25 cycles of 94°C for 30 s, 68°C for 30 s, 72°C for 4 min. The obtained 5′RACE products were gel excised, introduced into the pUC19 vector using in-fusion cloning, and sequenced by Sanger sequencing to detect the transcripts.

LUC reporter assays

For LUC reporter system assays in *N. benthamiana* leaves, a 1986-bp *RB* fragment including the intron structure was amplified from *RB* transgenic potato (SP951) genomic DNA and fused with *LUC* gene ligated into pCAMBIA1300. Four- or five-week-old *N. benthamiana* leaves were infiltrated with Agrobacterium strain GV3101 harboring the indicated constructs resuspended in infiltration buffer for 48 h, after which the leaves were sprayed with 1 mM D-luciferin substrate and incubated for 5 min in the dark. The sprayed leaves were photographed using a Tanon-5200 Multi Chemiluminescent Imaging System (Tanon, China). For quantification of LUC activity, *N. benthamiana* leaf discs were collected at 48 h after infiltration (hpi) and incubated with 1 mM D-luciferin in a 96-well plate, and LUC activity was quantified with the Promega GloMax Navigator microplate luminometer (Promega, USA).

Yeast two-hybrid screening

To identify interacting partners with the *P. infestans* effector IPI-O1, a yeast two-hybrid interaction screen was performed by Hybrigenics Services (Évry-Courouronnes, France) using IPI-O1 as a bait in an ULTImate Y2H library constructed from *N. benthamiana*. IPI-O1, encoding amino acids 2-132, was cloned into the inducible pB35 vector as a fusion with GAL4 at the amino terminus. The prey library was prepared in the proprietary pP6 Hybrigenics vector. A total of 81.6 million interactions were analyzed and 254 clones were processed by sequencing of the prey inserts. These prey fragments were fused out-of-frame with the Gal4 activation domain (AD) in pP6. However, *Saccharaomyces cerevisiae* are able to translate a percentage of the correct fusion proteins using ribosomal frameshift (Fromont-Racine et al., 1997; Vidal & Legrain, 1999). For this reason, it is possible to identify true interacting proteins from out-of-frame clones.

Hypersensitive response phenotype and ion leakage

Hypersensitive cell death during the ETI process was scored at 4 dpi and was quantified using an ion leakage assay (Mittler et al., 1999). Membrane ion leakage was determined by measuring electrolytes leaked from leaf discs. For each measurement, five 9 mm leaf discs were immersed in 5 mL distilled water at room temperature (22-25°C) for 3h. After which, the initial conductivity was measured with Multi-parameter tester (Mettler Toledo S400-K), referred to as value A. Total conductivity was determined after boiling at 95°C for 25 min and cooling to room temperature; this is referred to as value B. The ion leakage was expressed as the percentage of the initial conductivity versus the total conductivity (value A/value B) ×100%.

Transcription inhibition assay

Pladienolide B (CAS:445493-23-2) was purchased from Adooq. Pla-B, dissolved in DMSO, was infiltrated into *RB* transgenic *N. benthamiana*. The exact concentration of DMSO was used as control infiltrated in *N. benthamiana*.

Lanthanum (III) chloride ($LaCl_3$) (Sigma, CAS: 10099-58-8) was dissolved in water and infiltrated at a concentration of 2 mM.

Acknowledgements

We thank Prof. Jiamu Du, Porf. Zhe Wu (Southern University of Science and Technology), Prof. Jiming Jiang (Michigan State University), Prof. Sebastian Schornack (University of Cambridge), Prof. Yan Wang (Nanjing Agriculture University) for helpful discussions.

This work was supported by the Chinese National Science Funds Grants (32130088, 32102234) and the China Agriculture Research System-potato (CARS-potato, CARS-09-P20). This research was supported in part by the United States Department of Agriculture (USDA) Agricultural Research Service (ARS). Funding was provided through USDA National Institute of Food and Agriculture (NIFA) Plant-Associated Microbes and Plant-Microbe Interactions award number 2014-67013-21593. The findings and conclusions in this publication are those of the author(s) and should not be construed to represent any official USDA or United States Government determination or policy.

References

Axtell, M.J., and Staskawicz, B.J. (2003). Initiation of RPS2-specified disease resistance in Arabidopsis is coupled to the AvrRpt2-directed elimination of RIN4. Cell 112, 369-377.

Barta, A., Kalyna, M., and Lorković, Z.J. (2008). Plant SR Proteins and Their Functions. In Nuclear pre-mRNA Processing in Plants, A.S.N. Reddy and M. Golovkin, eds (Berlin, Heidelberg: Springer Berlin Heidelberg), pp. 83-102.

Bazin, J., Mariappan, K., Jiang, Y., Blein, T., Voelz, R., Crespi, M., and Hirt, H. (2020). Role of MPK4 in pathogen-associated molecular pattern-triggered alternative splicing in Arabidopsis. PLoS Pathog 16, e1008401.

Bhaskar, P.B., Raasch, J.A., Kramer, L.C., Neumann, P., Wielgus, S.M., Austin-Phillips, S., and Jiang, J. (2008). Sgt1, but not Rar1, is essential for the RB-mediated broad-spectrum resistance to potato late blight. BMC Plant Biol 8, 8.

Boevink, P.C., Wang, X., McLellan, H., He, Q., Naqvi, S., Armstrong, M.R., Zhang, W., Hein, I., Gilroy, E.M., and Tian, Z. (2016). A *Phytophthora infestans* RXLR effector targets plant PP1c isoforms that promote late blight disease. Nature Communications 7,

10311.

Bradeen, J.M., Iorizzo, M., Mollov, D.S., Raasch, J., Kramer, L.C., Millett, B.P., Austin-Phillips, S., Jiang, J., and Carputo, D. (2009). Higher copy numbers of the potato *RB* transgene correspond to enhanced transcript and late blight resistance levels. Molecular Plant-Microbe Interactions 22, 437-446.

Cesari, S., Bernoux, M., Moncuquet, P., Kroj, T., and Dodds, P.N. (2014). A novel conserved mechanism for plant NLR protein pairs: the "integrated decoy" hypothesis. Front Plant Sci 5, 606.

Champouret, N., Bouwmeester, K., Rietman, H., Lee, T.v.d., Maliepaard, C., Heupink, A., Vondervoort, P.J.I.v.d., Jacobsen, E., Visser, R.G.F., Vossen, E.A.G.v.d., Govers, F., and Vleeshouwers, V.G.A.A. (2009). *Phytophthora infestans* Isolates Lacking Class I *ipiO* Variants Are Virulent on *Rpi-blb1* Potato. MPMI 22, 1535-1545.

Chen, M., and Manley, J.L. (2009). Mechanisms of alternative splicing regulation: insights from molecular and genomics approaches. Nat Rev Mol Cell Biol 10, 741-754.

Chen, Y., Liu, Z., and Halterman, D.A. (2012). Molecular determinants of resistance activation and suppression by Phytophthora infestans effector IPI-O. PLoS Pathogen 8, e1002595.

Cheng, Y.T., Li, Y., Huang, S., Huang, Y., Dong, X., Zhang, Y., and Li, X. (2011). Stability of plant immune-receptor resistance proteins is controlled by SKP1-CULLIN1-F-box (SCF)-mediated protein degradation. Proc Natl Acad Sci U S A 108, 14694-14699.

Couto, D., and Zipfel, C. (2016). Regulation of pattern recognition receptor signalling in plants. Nat Rev Immunol 16, 537-552.

Cretu, C., Agrawal, A.A., Cook, A., Will, C.L., Fekkes, P., Smith, P.G., Luhrmann, R., Larsen, N., Buonamici, S., and Pena, V. (2018). Structural Basis of Splicing Modulation by Antitumor Macrolide Compounds. Mol Cell 70, 265-273 e268.

Cui, C., Wang, J.-J., Zhao, J.-H., Fang, Y.-Y., He, X.-F., Guo, H.-S., and Duan, C.-G. (2020). A Brassica miRNA Regulates Plant Growth and Immunity through Distinct Modes of Action. Mol. Plant 13, 231-245.

Cui, H., Tsuda, K., and Parker, J.E. (2015). Effector-Triggered Immunity: From Pathogen Perception to Robust Defense. Annual Review of Plant Biology 66, 487-511.

Dagdas, Y.F., Belhaj, K., Maqbool, A., Chaparro-Garcia, A., Pandey, P., Petre, B., Tabassum, N., Cruz-Mireles, N., Hughes, R.K., Sklenar, J., Win, J., Menke, F., Findlay, K., Banfield, M.J., Kamoun, S., and Bozkurt, T.O. (2016). An effector of the Irish potato famine pathogen antagonizes a host autophagy cargo receptor. Elife 5.

Dangl, J.L., and Jones, J.D.G. (2001). Plant pathogens and integrated defence responses to infection. Nature 411, 826-833.

Deng, Y., Zhai, K., Xie, Z., Yang, D., Zhu, X., Liu, J., Wang, X., Qin, P., Yang, Y., Zhang, G., Li, Q., Zhang, J., Wu, S., Milazzo, J., Mao, B., Wang, E., Xie, H., Tharreau, D., and He, Z. (2019). Epigenetic regulation of antagonistic receptors confers rice blast resistance with yield balance. Science 355, 962-965.

Dinesh-Kumar, S.P., and Baker, B.J. (2000). Alternatively spliced N resistance gene transcripts: Their possible role in tobacco mosaic virus resistance. Proc. Natl Acad. Sci. USA 97, 1908–1913.

Dinh, H.X., Singh, D., Gomez de la Cruz, D., Hensel, G., Kumlehn, J., Mascher, M., Stein, N., Perovic, D., Ayliffe, M., Moscou, M.J., Park, R.F., and Pourkheirandish, M. (2022). The barley leaf rust resistance gene *Rph3* encodes a predicted membrane protein and is induced upon infection by avirulent pathotypes of *Puccinia hordei*. Nature Communications 13, 2386.

Dodds, P.N., and Rathjen, J.P. (2010). Plant immunity: towards an integrated view of plant-pathogen interactions. Nature reviews. Genetics 11, 539-548.

Dodds, P.N., Lawrence, G.J., Catanzariti, A.-M., Teh, T., Wang, C.-I.A., Ayliffe, M.A., Kobe, B., and Ellis, J.G. (2006). Direct protein interaction underlies gene-for-gene specificity and coevolution of the flax resistance genes and flax rust avirulence genes. Proceedings of the National Academy of Sciences 103, 8888-8893.

Duxbury, Z., Wu, C.H., and Ding, P. (2021). A Comparative Overview of the Intracellular Guardians of Plants and Animals: NLRs in Innate Immunity and Beyond. Annu Rev Plant Biol 72, 155-184.

Filichkin, S.A., Priest, H.D., Givan, S.A., Shen, R., Bryant, D.W., Fox, S.E., Wong, W.-K., and Mockler, T.C. (2010). Genome-wide mapping of alternative splicing in Arabidopsis thaliana. Genome Research 20, 45-58.

Gao, M., He, Y., Yin, X., Zhong, X., Yan, B., Wu, Y., Chen, J., Li, X., Zhai, K., Huang, Y., Gong, X., Chang, H., Xie, S., Liu, J., Yue, J., Xu, J., Zhang, G., Deng, Y., Wang, E., Tharreau, D., Wang, G.L., Yang, W., and He, Z. (2021a). Ca(2+) sensor-mediated ROS scavenging suppresses rice immunity and is exploited by a fungal effector. Cell 184, 5391-5404 e5317.

Gao, W., Liu, Y., Huang, J., Chen, Y., Chen, C., Lu, L., Zhao, H., Men, S., and Zhang, X. (2021b). MES7 Modulates Seed Germination via Regulating Salicylic Acid Content in Arabidopsis. Plants (Basel) 10.

Halterman, D., Wei, F., and Wise, R. (2003). Powdery mildew induced *Mla* mRNAs are alternatively spliced and contain multiple upstream open reading frames. Plant Physiol 131, 558-567.

Halterman, D.A., and Wise, R.P. (2006). Upstream open reading frames of the barley Mla13 powdery mildew resistance gene function co-operatively to down-regulate translation. Molecular Plant Pathology 7, 167-176.

Haverkort, A.J., Struik, P.C., Visser, R.G.F., and Jacobsen, E. (2009). Applied Biotechnology to Combat Late Blight in Potato Caused by Phytophthora Infestans. Potato Research 52, 249-264.

He, Z., Webster, S., and He, S.Y. (2022). Growth-defense trade-offs in plants. Current Biology 32, R634-R639.

Huang, C.Y., Rangel, D.S., Qin, X., Bui, C., Li, R., Jia, Z., Cui, X., and Jin, H. (2021). The chromatin-remodeling protein BAF60/SWP73A regulates the plant immune receptor NLRs. Cell Host Microbe 29, 425-434 e424.

Huang, J., Lu, X., Wu, H., Xie, Y., Peng, Q., Gu, L., Wu, J., Wang, Y., Reddy, A.S.N., and Dong, S. (2020). *Phytophthora* effectors modulate genome-wide alternative splicing of host mRNAs to reprogram plant immunity. Molecular plant 13, 1470-1484.

Huang, J., Gu, L., Zhang, Y., Yan, T., Kong, G., Kong, L., Guo, B., Qiu, M., Wang, Y., Jing, M., Xing, W., Ye, W., Wu, Z., Zhang, Z., Zheng, X., Gijzen, M., Wang, Y., and Dong, S. (2017). An oomycete plant pathogen reprograms host pre-mRNA splicing to subvert immunity. Nature Communications 8.

Jia, J., Long, Y., Zhang, H., Li, Z., Liu, Z., Zhao, Y., Lu, D., Jin, X., Deng, X., Xia, R., Cao,

X., and Zhai, J. (2020). Post-transcriptional splicing of nascent RNA contributes to widespread intron retention in plants. Nature Plants 6, 780-788.

Jones, J.D., and Dangl, J.L. (2006). The plant immune system. Nature 444, 323-329.

Jung, H.W., Panigrahi, G.K., Jung, G.Y., Lee, Y.J., Shin, K.H., Sahoo, A., Choi, E.S., Lee, E., Man Kim, K., Yang, S.H., Jeon, J.S., Lee, S.C., and Kim, S.H. (2020). Pathogen-associated molecular pattern-triggered immunity involves proteolytic degradation of core nonsense-mediated mRNA decay factors during the early defense response. Plant Cell 32, 1081-1101.

Kamoun, S., and Smart, C.D. (2005). Late Blight of Potato and Tomato in the Genomics Era. Plant Disease 89, 692-699.

Kamoun, S., Furzer, O., Jones, J.D.G., Judelson, H.S., Ali, G.S., Dalio, R.J.D., Roy, S.G., Schena, L., Zambounis, A., Panabieres, F., Cahill, D., Ruocco, M., Figueiredo, A., Chen, X.R., Hulvey, J., Stam, R., Lamour, K., Gijzen, M., Tyler, B.M., Grunwald, N.J., Mukhtar, M.S., Tome, D.F.A., Tor, M., Van den Ackerveken, G., McDowell, J., Daayf, F., Fry, W.E., Lindqvist-Kreuze, H., Meijer, H.J.G., Petre, B., Ristaino, J., Yoshida, K., Birch, P.R.J., and Govers, F. (2015). The Top 10 oomycete pathogens in molecular plant pathology. Molecular Plant Pathology 16, 413-434.

Karki, H.S., Jansky, S.H., and Halterman, D.A. (2021). Screening of Wild Potatoes Identifies New Sources of Late Blight Resistance. Plant Disease 105, 368-376.

Katou, S., Yoshioka, H., Kawakita, K., Rowland, O., Jones, J.D.G., Mori, H., and Doke, N. (2005). Involvement of PPS3 Phosphorylated by Elicitor-Responsive Mitogen-Activated Protein Kinases in the Regulation of Plant Cell Death. Plant Physiology 139, 1914-1926.

Klepikova, A.V., Kasianov, A.S., Gerasimov, E.S., Logacheva, M.D., and Penin, A.A. (2016). A high resolution map of the Arabidopsis thaliana developmental transcriptome based on RNA-seq profiling. The Plant Journal 88, 1058-1070.

Kotake, Y., Sagane, K., Owa, T., Mimori-Kiyosue, Y., Shimizu, H., Uesugi, M., Ishihama, Y., Iwata, M., and Mizui, Y. (2007). Splicing factor SF3b as a target of the antitumor natural product pladienolide. Nat Chem Biol 3, 570-575.

Lai, Y., and Eulgem, T. (2018). Transcript-level expression control of plant NLR genes. Mol

Plant Pathol 19, 1267-1281.

Li, F., Pignatta, D., Bendix, C., Brunkard, J.O., Cohn, M.M., Tung, J., Sun, H., Kumar, P., and Baker, B. (2012). MicroRNA regulation of plant innate immune receptors. Proceedings of the National Academy of Sciences USA 109, 1790-1795.

Li, X., Kapos, P., and Zhang, Y. (2015). NLRs in plants. Curr Opin Immunol 32, 114-121.

Liao, S.E., and Regev, O. (2021). Splicing at the phase-separated nuclear speckle interface: a model. Nucleic Acids Res 49, 636-645.

Liu, N., Hake, K., Wang, W., Zhao, T., Romeis, T., and Tang, D. (2017). CALCIUM-DEPENDENT PROTEIN KINASE5 Associates with the Truncated NLR Protein TIR-NBS2 to Contribute to exo70B1-Mediated Immunity. Plant Cell 29, 746-759.

Long, Jennifer C., and Caceres, Javier F. (2008). The SR protein family of splicing factors: master regulators of gene expression. Biochemical Journal 417, 15-27.

Lu, Q., Tang, X., Tian, G., Wang, F., Liu, K., Nguyen, V., Kohalmi, S.E., Keller, W.A., Tsang, E.W.T., Harada, J.J., Rothstein, S.J., and Cui, Y. (2010a). Arabidopsis homolog of the yeast TREX-2 mRNA export complex: components and anchoring nucleoporin. The Plant Journal 61, 259-270.

Lu, T., Lu, G., Fan, D., Zhu, C., Li, W., Zhao, Q., Feng, Q., Zhao, Y., Guo, Y., Li, W., Huang, X., and Han, B. (2010b). Function annotation of the rice transcriptome at single-nucleotide resolution by RNA-seq. Genome Research 20, 1238-1249.

Maqbool, A., Saitoh, H., Franceschetti, M., Stevenson, C.E., Uemura, A., Kanzaki, H., Kamoun, S., Terauchi, R., and Banfield, M.J. (2015). Structural basis of pathogen recognition by an integrated HMA domain in a plant NLR immune receptor. Elife 4.

Marquez, Y., Brown, J.W.S., Simpson, C., Barta, A., and Kalyna, M. (2012). Transcriptome survey reveals increased complexity of the alternative splicing landscape in Arabidopsis. Genome Research 22, 1184-1195.

Ning, Y., Liu, W., and Wang, G.L. (2017). Balancing Immunity and Yield in Crop Plants. Trends Plant Sci 22, 1069-1079.

Nishimura, M.T., Anderson, R.G., Cherkis, K.A., Law, T.F., Liu, Q.L., Machius, M., Nimchuk, Z.L., Yang, L., Chung, E.H., El Kasmi, F., Hyunh, M., Osborne Nishimura,

E., Sondek, J.E., and Dangl, J.L. (2017). TIR-only protein RBA1 recognizes a pathogen effector to regulate cell death in Arabidopsis. Proceedings of the National Academy of Sciences USA 114, E2053-E2062.

Ofir, G., Herbst, E., Baroz, M., Cohen, D., Millman, A., Doron, S., Tal, N., Malheiro, D.B.A., Malitsky, S., Amitai, G., and Sorek, R. (2021). Antiviral activity of bacterial TIR domains via immune signalling molecules. Nature 600, 116-120.

Palma, K., Zhao, Q., Cheng, Y.T., Bi, D., Monaghan, J., Cheng, W., Zhang, Y., and Li, X. (2007). Regulation of plant innate immunity by three proteins in a complex conserved across the plant and animal kingdoms. Genes & Development 21, 1484-1493.

Paluchowska, P., Sliwka, J., and Yin, Z. (2022). Late blight resistance genes in potato breeding. Planta 255, 127.

Reddy, A.S. (2007). Alternative splicing of pre-messenger RNAs in plants in the genomic era. Annu Rev Plant Biol 58, 267-294.

Reddy, A.S.N. (2004). Plant serine/arginine-rich proteins and their role in pre-mRNA splicing. Trends in Plant Science 9, 541-547.

Reddy, A.S.N., Marquez, Y., Kalyna, M., and Barta, A. (2013a). Complexity of the Alternative Splicing Landscape in Plants. The Plant Cell 25, 3657-3683.

Reddy, A.S.N., Marquez, Y., Kalyna, M., and Barta, A. (2013b). Complexity of the Alternative Splicing Landscape in Plants The Plant Cell 25, 3657-3683.

Reddy, A.S.N., Huang, J., Syed, N.H., Ben-Hur, A., Dong, S., and Gu, L. (2020). Decoding co-/post-transcriptional complexities of plant transcriptomes and epitranscriptome using next-generation sequencing technologies. Biochemical Society Transactions 48, 2399-2414.

Sanchez-Martin, J., Widrig, V., Herren, G., Wicker, T., Zbinden, H., Gronnier, J., Sporri, L., Praz, C.R., Heuberger, M., Kolodziej, M.C., Isaksson, J., Steuernagel, B., Karafiatova, M., Dolezel, J., Zipfel, C., and Keller, B. (2021). Wheat Pm4 resistance to powdery mildew is controlled by alternative splice variants encoding chimeric proteins. Nat Plants 7, 327-341.

Sarris, P.F., Duxbury, Z., Huh, S.U., Ma, Y., Segonzac, C., Sklenar, J., Derbyshire, P., Cevik, V., Rallapalli, G., Saucet, S.B., Wirthmueller, L., Menke, F.L.H., Sohn, K.H., and

Jones, J.D.G. (2015). A Plant Immune Receptor Detects Pathogen Effectors that Target WRKY Transcription Factors. Cell 161, 1089-1100.

Sheth, N., Roca, X., Hastings, M.L., Roeder, T., Krainer, A.R., and Sachidanandam, R. (2006). Comprehensive splice-site analysis using comparative genomics. Nucleic Acids Res 34, 3955-3967.

Slane, D., Lee, C.H., Kolb, M., Dent, C., Miao, Y., Franz-Wachtel, M., Lau, S., Macek, B., Balasubramanian, S., Bayer, M., and Jurgens, G. (2020). The integral spliceosomal component CWC15 is required for development in Arabidopsis. Sci Rep 10, 13336.

Song, J., Bradeen, J.M., Naess, S.K., Raasch, J.A., Wielgus, S.M., Haberlach, G.T., Liu, J., Kuang, H., Austin-Phillips, S., Buell, C.R., Helgeson, J.P., and Jiang, J. (2003). Gene RB cloned from Solanum bulbocastanum confers broad spectrum resistance to potato late blight. Proc Natl Acad Sci U S A 100, 9128-9133.

Stam, M., Mol, J.N.M., and Kooter, J.M. (1997). The silence of genes in transgenic plants. Annals of Botany 79, 3-12.

Sukarta, O.C.A., Zheng, Q., Slootweg, E.J., Mekken, M., Mendel, M., Putker, V., Bertran, A., Brand, A., Overmars, H., Pomp, R., Roosien, J., Boeren, S., Smant, G., and Goverse, A. (2022). GLYCINE-RICH RNA-BINDING PROTEIN 7 potentiates effector-triggered immunity through an RNA recognition motif. Plant Physiol 189, 972-987.

Sun, H., Jiao, W.B., Krause, K., Campoy, J.A., Goel, M., Folz-Donahue, K., Kukat, C., Huettel, B., and Schneeberger, K. (2022). Chromosome-scale and haplotype-resolved genome assembly of a tetraploid potato cultivar. Nat Genet 54, 342-348.

Tsuchiya, T., and Eulgem, T. (2013). An alternative polyadenylation mechanism coopted to the Arabidopsis RPP7 gene through intronic retrotransposon domestication. Proceedings of the National Academy of Sciences USA 110, E3535-3543.

Van de Weyer, A.L., Monteiro, F., Furzer, O.J., Nishimura, M.T., Cevik, V., Witek, K., Jones, J.D.G., Dangl, J.L., Weigel, D., and Bemm, F. (2019). A Species-Wide Inventory of NLR Genes and Alleles in Arabidopsis thaliana. Cell 178, 1260-1272 e1214.

van der Hoorn, R.A., and Kamoun, S. (2008). From Guard to Decoy: a new model for perception of plant pathogen effectors. Plant Cell 20, 2009-2017.

van der Vossen, E., Sikkema, A., Hekkert, B., Gros, J., Stevens, P., Muskens, M., Wouters, D., Pereira, A., Stiekema, W., and Allefs, S. (2003). An ancient R gene from the wild potato species Solanum bulbocastanum confers broad-spectrum resistance to Phytophthora infestans in cultivated potato and tomato. Plant J 36, 867-882.

Vleeshouwers, V.G., Rietman, H., Krenek, P., Champouret, N., Young, C., Oh, S.K., Wang, M., Bouwmeester, K., Vosman, B., Visser, R.G., Jacobsen, E., Govers, F., Kamoun, S., and Van der Vossen, E.A. (2008). Effector genomics accelerates discovery and functional profiling of potato disease resistance and phytophthora infestans avirulence genes. PLoS One 3, e2875.

Wan, R., Bai, R., Zhan, X., and Shi, Y. (2020). How Is Precursor Messenger RNA Spliced by the Spliceosome? Annu Rev Biochem 89, 333-358.

Wang, G., Roux, B., Feng, F., Guy, E., Li, L., Li, N., Zhang, X., Lautier, M., Jardinaud, M.F., Chabannes, M., Arlat, M., Chen, S., He, C., Noel, L.D., and Zhou, J.M. (2015). The Decoy Substrate of a Pathogen Effector and a Pseudokinase Specify Pathogen-Induced Modified-Self Recognition and Immunity in Plants. Cell Host Microbe 18, 285-295.

Wang, J., Hu, M., Wang, J., Qi, J., Han, Z., Wang, G., Qi, Y., Wang, H.W., Zhou, J.M., and Chai, J. (2019). Reconstitution and structure of a plant NLR resistosome conferring immunity. Science 364.

Wang, L., Yang, T., Wang, B., Lin, Q., and Yu, F. (2020). RALF1-FERONIA complex affects splicing dynamics to modulate stress responses and growth in plants. Science Advances 6, eaaz1622.

Wang, S., McLellan, H., Bukharova, T., He, Q., Murphy, F., Shi, J., Sun, S., van Weymers, P., Ren, Y., Thilliez, G., Wang, H., Chen, X., Engelhardt, S., Vleeshouwers, V., Gilroy, E.M., Whisson, S.C., Hein, I., Wang, X., Tian, Z., Birch, P.R.J., and Boevink, P.C. (2018). Phytophthora infestans RXLR effectors act in concert at diverse subcellular locations to enhance host colonization. Journal of Experimental Botany 70, 343-356.

Wu, Z., Zhu, D., Lin, X., Miao, J., Gu, L., Deng, X., Yang, Q., Sun, K., Zhu, D., Cao, X., Tsuge, T., Dean, C., Aoyama, T., Gu, H., and Qu, L.J. (2016). RNA Binding Proteins RZ-1B and RZ-1C Play Critical Roles in Regulating Pre-mRNA Splicing and Gene

Expression during Development in Arabidopsis. Plant Cell 28, 55-73.

Xu, F., Xu, S., Wiermer, M., Zhang, Y., and Li, X. (2012). The cyclin L homolog MOS12 and the MOS4-associated complex are required for the proper splicing of plant resistance genes. The plant jouranl 70, 916-928.

Xu, S., Zhang, Z., Jing, B., Gannon, P., Ding, J., Xu, F., Li, X., and Zhang, Y. (2011). Transportin-SR is required for proper splicing of resistance genes and plant immunity. PLOS Genetics 7, e1002159.

Yang, S., Tang, F., and Zhu, H. (2014). Alternative splicing in plant immunity. International journal of molecular sciences 15, 10424-10445.

Zhang, F., Fang, H., Wang, M., He, F., Tao, H., Wang, R., Long, J., Wang, J., Wang, G.L., and Ning, Y. (2022). APIP5 functions as a transcription factor and an RNA-binding protein to modulate cell death and immunity in rice. Nucleic Acids Res 50, 5064-5079.

Zhang, X.-C., and Gassmann, W. (2007). Alternative splicing and mRNA levels of the disease resistance gene *RPS4* are induced during defense responses. Plant Physiology 145, 1577-1587.

Zhang, Y., and Li, X. (2005). A putative nucleoporin 96 is required for both basal defense and constitutive resistance responses mediated by *suppressor of npr1-1, constitutive 1*. The Plant Cell 17, 1306-1316.

Zhang, Y., Xu, S., Ding, P., Wang, D., Cheng, Y.T., He, J., Gao, M., Xu, F., Li, Y., Zhu, Z., Li, X., and Zhang, Y. (2010). Control of salicylic acid synthesis and systemic acquired resistance by two members of a plant-specific family of transcription factors. Proc Natl Acad Sci U S A 107, 18220-18225.

Zhao, J., and Song, J. (2021). NLR immune receptor RB is differentially targeted by two homologous but functionally distinct effector proteins. Plant Communications 2.

Zhou, J.-M., and Chai, J. (2008). Plant pathogenic bacterial type III effectors subdue host responses. Current Opinion in Microbiology 11, 179-185.

Figure Legends

Figure 1. The *RB* intron is alternatively spliced.

(A) Gene model and splicing isoforms of *RB*. 5' and 3' UTRs are shaded grey. The intron is denoted by a black line. The asterisk shows the location of a premature termination codon. The arrows indicate the primers used in (B). Red letters in *RB_IVS* denote mutations to change the intron splicing recognition sites. **(B)** RT-PCR of *RB* and *RB_IVS* splicing mutant from transgenic *S. tuberosum* cv. Favorita and transgenic *N. benthamiana*. *RB_IR* is 995bp, and *RB_CDS* is 316bp. cDNA of Favorita and wildtype *N. benthamiana* were used as negative controls. *StEF1α* and *NbEF1α* were used as internal controls. **(C)** Diagrams showing the domains present in each of the predicted proteins produced from transcripts. **(D)** Expression of Myc-tagged fusions of RB, RB_CDS, and RB_IR in *N. benthamiana* was confirmed by western blotting using an anti-Myc antibody. The asterisk stands for the predicted protein RB RB_CDS and RB_IR. Equal protein loading was visualized by Ponceau S staining.

Figure 2. *RB* intron splicing is specifically induced following *P. infestans* inoculation.

(A) RT-PCR of *RB_IR* or *RB_CDS* variants in *RB* transgenic potato following inoculation with water (mock), *P. infestans* JH19 or *P. capsici* LT1534. *StEF1α* was used as the internal control. **(B)** Splicing ratio of *RB* in transgenic potato following inoculation with water (mock), *P. infestans* JH19, or *P. capsici* LT1534. Transcript levels were detected by RT-qPCR and normalized to *RB_CDS* following mock treatment at 0 dpi. Bars represent the mean ± SD from three independent replicates. ns, no significant difference. One asterisk denotes a significant difference at $P<0.05$, and three asterisks denotes a significant difference at $P<0.001$ using a two-way ANOVA with Tukey's test.

Figure 3. Intron retention in *RB* results in susceptibility to *P. infestans*.

(A) Zoospore suspension of *P. infestans* strain JH19 was used to inoculate *RB*, *RB_CDS*, *RB_IR* and *RB_IVS* transgenic potato plants at a concentration of 15,000 zoospores/mL. Plants were photographed at 5 dpi. The numbers represent the ratio of resistant plants compared to all inoculated plants. Bar = 5 cm. **(B)** Zoospore suspension of *P. infestans* strain

JH19 was drop-inoculated on detached leaves of *RB* transgenic potato expressing the indicated gene variants. The infected leaves were photographed at 4 dpi. The numbers represent the ratio of resistant leaves compared to all inoculated leaves. Bars represent the percent infected area of the detached leaves. The data represents the mean ± SD from 12 replications. Different letters above bars denote a significant difference at P<0.001 using a two-way ANOVA with Dunn's test.

Figure 4. Spliceosome activity is necessary for *RB*-mediated resistance to *P. infestans*.

(A) Trypan blue staining of *RB* transgenic *N. benthamiana* following agroinfiltration of RNAi-hairpin constructs and inoculation with *P. infestans* zoospores. EV = empty vector control. Leaves were photographed at 5 dpi. **(B)** Lesion areas (cm^2) of inoculated leaves in (A). Data represents the mean ± SD from 8 replicates. Different letters above bars denotes a significant difference at P<0.001 using a one-way ANOVA with Dunn's test. **(C)** Splicing ratio of *RB* in *RB* transgenic *N. benthamiana* following agroinfiltration of RNAi-hairpin constructs for 1 day and inoculation with *P. infestans* zoospores. RNA was extracted 2 days after pathogen inoculation. Transcript levels were detected by RT-qPCR and normalized to *RB_CDS* in RNAi-EV and following mock treatment. Bars represent the mean ± SD in three independent replicates. **(D)** Agroinfiltration of IPI-O1 in *RB* and *RB_CDS* transgenic *N. benthamiana* with DMSO (control), 1 μM splicing modulator Pladienolide B (Pla-B), or 30 μM Pla-B. Cell death was visually assessed and photographed at 4 dpi (left). Numbers show the ratio of infiltrated areas with cell death compared to the all infiltrated areas. Electrolyte leakage was monitored by conductivity measurements following the same treatments (right). Data represents the mean ± SD from 8 replications. **(E)** Splicing ratio of *RB* in *RB* transgenic *N. benthamiana* following treatment with DMSO (control), 1 μM Pla-B, or 30 μM Pla-B and inoculation with *P. infestans* zoospores at 2 dpi by RT-qPCR. ns, no significant difference. Three asterisks denotes a statistical difference at P<0.001 using a two-way ANOVA with Tukey's test.

Figure 5. IPI-O1 induces *RB* intron splicing.

(A) Schematic diagram of the *RB_LUC* alternative splicing reporter system. The genomic

sequence of *RB* was fused with the luciferase (*LUC*) gene to construct 35S::*RB-LUC*. Intron retention introduces a premature termination codon (PTC) and no production of the luciferase reporter. Intron splicing leads to a full-length RB-LUC protein with luciferase activity. The *35S*::*RB_CDS-LUC* construct with the intron removed produces a full-length RB-LUC protein with luciferase activity regardless of intron splicing activity. The *35S*::*LUC* construct is a positive control. **(B)** Results of co-expression of the reporters with multiple splicing regulatory effectors (SRE) that we previously identified (Huang et al., 2020). LUC activity was quantified at 48 hpi. Relative LUC activity was normalized to the activity of the *35S*::*RB_CDS-LUC* construct with mock treatment. Data represents the mean ± SD from 24 replications. Different letters above each bar represent a significant difference at P<0.001 using a two-way ANOVA with Dunn's test. **(C)** GFP-tagged SRE fusion protein expression in *N. benthamiana* was confirmed by western blotting using an anti-GFP antibody. Protein loading was visualized by Ponceau S staining.

Figure 6. Nuclear localization of IPI-O1 is necessary for *RB* intron splicing.

(A) Schematic diagrams at the top show the location of alanine replacements within the nuclear localization signal of IPI-O1. GFP-IPI-O1 and GFP-IPI-O1^{nls} were expressed in *N. benthamiana* leaves for 48 h before imaging, Scale bar = 20 μm. **(B)** Subcellular localization of IPI-O1 and IPI-O1^{nls}. Bars represent the number of times that GFP was detected in the nucleoplasm or nucleolus following infiltration of GFP-IPI-O1 and GFP-IPI-O1^{nls}. Data represents the mean ± SD of three replicates. **(C)** Expression of GFP-tagged fusions of IPI-O1 and IPI-O1^{nls} in *N. benthamiana* was confirmed by protein blotting using an anti-GFP antibody. Protein loading was visualized by Ponceau S staining. **(D)** On the left are visual examples and incidence ratios of hypersensitive cell death responses following agroinfiltration of IPI-O1 and IPI-O1^{nls} in leaves of *RB*, *RB_CDS*, and *RB_IR* transgenic *N. benthamiana*. Cell death was visually assessed and photographed at 4 dpi. The right panel shows results of electrolyte leakage assays of infiltrated areas. Data represents the mean ± SD of 12 replications. **(E)** Splicing ratio of *RB* in *RB* transgenic *N. benthamiana* following agroinfiltration of IPI-O1 and IPI-O1^{nls} at 2 dpi by RT-qPCR. Bars represent the mean ± SD of three independent replicates. **(F)** Results of co-expression of RB_LUC reporters with

mock, GFP, IPI-O1 and IPI-O1^{nls} in *N. benthamiana* leaves by agroinfiltration. LUC activity was quantified at 2 dpi. Relative LUC activity was normalized to the activity of the 35S::*LUC* construct with mock treatment. Data represents the mean ± SD of 30 replications. For all graphs, ns = no significant difference and three asterisks denotes a statistical difference at P<0.001 using a two-way ANOVA with Tukey's test.

Figure 7. IPI-O1 physically interacts with splicing factor CWC15.

(A) Yeast-two hybrid interaction between IPI-O1 and CWC15 homologs from *N. benthamiana*. Yeast transformants were spotted as 10-fold serial dilutions on SD medium without leucine and tryptophan (SD–2), or without histidine, leucine, adenine, and tryptophan (SD–4). Yeast cells were photographed 2-3 days after plating. Empty BD and AD plasmids (EV) were used as controls. Experiments were performed at least three times with similar results. **(B)** Immunoprecipitation (IP) of StCWC15a/b-GFP with RFP-IPI-O1, RFP-IPI-O1^{nls}, or RFP-Pi04314 following agroinfiltration in *N. benthamiana* leaves. Expression of constructs in the leaves is indicated by +. Markers are indicated on the right, and the Ponceau S stain was used to show levels of protein loading. **(C)** *In vitro* pull-down assay using the GST-tagged StCWC15a/b to immunoprecipitate IPI-O1 or IPI-O1^{nls}. Input and GST-pull-down proteins were visualized by protein blotting using anti-GST and anti-His antibodies. Asterisks (*) indicate the protein bands that correspond to the expected size of CWC15a/b. **(D)** IPI-O1, but not IPI-O1^{nls}, can interact with CWC15 homologs in potato. Yeast transformants were spotted as 10-fold serial dilutions on SD medium without leucine and tryptophan (SD–2), or without histidine, leucine, adenine, and tryptophan (SD–4). Yeast cells were photographed 2-3 days later. BD and AD are bait and prey EVs, respectively. Experiments were performed at least three times with similar results. **(E)** IPI-O1 co-localizes with StCWC15a/b in nuclear speckles and the nucleolus. GFP-IPI-O1, GFP-IPI-O1^{nls}, and GFP alone were transiently co-expressed with StCWC15a/b-RFP by agroinfiltration in *N. benthamiana*. The left image is from the GFP channel, the middle image is from the RFP channel, and the right image is the overlay of the GFP and RFP channels. Numbers represent the frequency of cells showing indicated StCWC15 subcellular localization compared to the total StCWC15-positive cells in 25mm^2 discs from three biological replicates. Graphs show

the fluorescence intensity profiles across the arrows in the merged images. Bar = 5μm.

Figure 8. Silencing *StCWC15* disrupts *RB*-mediated resistance.

(A) Whole plants were spray-inoculated (left) and detached leaves were drop-inoculated (right) with zoospores of *P. infestans* strain JH19 in *RB* and *RB-StCWC15* RNAi transgenic potato. Bar = 3 cm. The number represents the frequency of leaves showing resistance compared to all inoculated leaves. **(B)** Zoospore suspension of *P. infestans* strain JH19 was drop-inoculated on detached leaves of *RB* and *RB-StCWC15* RNAi transgenic potato. The infected leaves were photographed at 4 dpi. The numbers represent the ratio of resistant leaves compared to all inoculated leaves. **(C)** Relative expression of *StCWC15a/b* in three RNAi transformed lines compared to *RB* transgenic potato. Bars represent the mean ± SD of three independent replicates. Three asterisks designate a statistical difference from the *RB* control at P<0.001 using a two-way ANOVA with Tukey's test. **(D)** Infection ratio of *P. infestans* JH19 on *RB* and *RB-StCWC15* RNAi transgenic potato lines. Data represents the mean ± SD from 10 replications. Different letters denote a significance difference at P<0.001 using a one-way ANOVA with Dunn's test. **(E)** Splicing ratio of *RB* in *RB-StCWC15* RNAi transgenic potato line #2 following inoculation with *P. infestans* zoospores at 2 dpi by RT-qPCR. Bars represent the mean ± SD from three independent replicates. ns=no significant difference and three asterisks denotes a statistical difference at P<0.001 using a two-way ANOVA with Tukey's test. **(F)** *NbCWC15* was silenced by VIGS in *RB*, *RB_CDS*, and *Rpi_blb2* transgenic *N. benthamiana* and inoculated with *P. infestans* JH19 on detached leaves. Photos (top) and lesion areas (bottom) were recorded at 5 dpi. Lesion area data represents the mean ± SD from 18 replications. **(G)** Complementation of *RB* function caused by *CWC15* silencing in *N. benthamiana* via synthetic *StCWC15* constructs (*StCWC15a/b*^{syn}). Agrobacterium expressing *StCWC15a/b*^{syn} constructs were infiltrated into *NbCWC15* silenced *RB* transgenic *N. benthmiana*, then inoculated with *P. infestans* JH19 zoospores. Photos and lesion areas were recorded at 5 dpi. Data represent the mean ± SD from 8 replications. Different letters denote a significance difference at P<0.001 using one-way ANOVA with Dunn's test.

Figure 9. Alternative intron splicing of *RB* balances plant growth and immunity.

(A) Photos of 21-day-old wild-type (WT) Favorita and *RB*, *RB_CDS*, and *RB_IR* transgenic tissue culture plants. Bar = 1 cm. **(B)** Average stem height and root length measurements of Favorita (WT) and 21-day-old transgenic potato tissue culture plants. Bars represent the mean ± SD from 15 tissue culture plants. **(C)** Tubers of Favorita (WT) and transgenic plants. Tubers were harvested and photographed 8 to 10 weeks after tissue culture plants were transplanted. Bar = 1 cm. **(D)** Average tuber yield, average individual tuber mass, and average number of tubers from greenhouse grown plants. Measurements were taken at 8 to 10 weeks after tissue culture plants were transplanted. Bars represent the mean ± SD from 15 replications of 3 independent lines for each genotype. **(E)** Total salicylic acid (SA) content in Favorita (WT) and transgenic *RB* and *RB_CDS* lines without pathogen inoculation. FW, fresh weight. Bars represent the mean ± SD from three independent replicates. **(F-G)** Relative expression of *SARD1* (F) and *PR1* (G) in the indicated transgenic potato as determined by RT-qPCR. Bars represent the mean ± SD from three independent replicates. For all graphs, different letters represent a statistical difference at $P<0.001$ using one-way ANOVA with Dunn's test.

Fig.10 Schematic model of the *P. infestans*-host pathosystem related to resistance gene *RB* and effector IPI-O1.

During normal growth (left), CWC15 proteins (grey triangles) are maintained in the nucleoplasm and *RB* transcripts exist primarily with the intron retained (*RB_IR*). This results in the production of a truncated, non-functional RB protein that supports growth over immunity. Following *P. infestans* infection, effector IPI-O1 is introduced into the plant cell and translocated to the nucleus, leading to a re-localization of CWC15 from the nucleoplasm to the nucleolus and speckles. This results in increased splicing of the *RB* intron (*RB_CDS*), resulting in production of a full-length RB protein that can elicit immunity.

Supplemental Figure S1. ***RB* undergoes AS and produces two transcript isoforms.** Schematic of two transcripts of *RB* amplified using 5′-rapid amplification of cDNA ends (5′-RACE). UPM primer is Universal Primer A Mix, GSP primer is gene specific primer of

RB. The white vertical lines represent single nucleotide polymorphisms that appeared in the sequencing results.

Supplemental Figure S2. ***RB* intron splicing is induced following *P. infestans* inoculation.**
(A) The relative transcription level of *RB* is modified following *P. infestans* but not *P. capsici* inoculation. Quantitative PCR with reverse transcription (RT–qPCR) analysis was performed using isoform-specific primers (Supplemental Data Set S2) to measure the transcript levels of two isoforms. **(B)** Total *RB* transcription levels do not change significantly during infection. RT–qPCR analysis was performed using primers (Supplemental Data Set S2) located in Exon1. For all graphs, bars represent the mean ± SD from three independent replicates. ns = no significant difference and three asterisks denotes a statistical difference at P<0.001 using a two-way ANOVA with Tukey's test.

Supplemental Figure S3. Intron retention in *RB* results in susceptibility to *P. infestans*.
(A) Zoospores of *P.infestans* strain JH19 were inoculated on detached transgenic *N. benthamiana* leaves expressing the indicated gene variants. On the top, leaves were stained with trypan blue and photographed at 5 dpi. Below, lesion areas were calculated using Image J. Data represents the mean ± SD from 21 inoculations from three independent experimental replicates. Different shapes indicate biological replicates. **(B)** Indicated transgenic *N. benthamiana* leaves were agroinfiltrated with IPI-O1 or GFP. On the top, cell death was visually assessed and photographed at 4dpi. The numbers represent incidence ratios of hypersensitive cell death responses. Below shows results of electrolyte leakage assays of infiltrated areas. Data represents the mean ± SD from 9 replications. For all graphs, different letters above each bar represent a statistical difference at P<0.001 using a two-way ANOVA with Dunn's test.

Supplemental Figure S4. Spliceosome activity is necessary for *RB*-mediated resistance to *P. infestans*.
(A) Agroinfiltrations of the indicated RNAi-hairpin constructs to silence *U1-70K*, *SF3B1* and

GRP7 in *N. benthamiana*, followed by co-agroinfiltration of the indicated *Avr/R* gene combinations. Cell death was visually assessed and photographed at 4 dpi. The numbers represent incidence ratios of hypersensitive cell death responses. **(B)** Electrolyte leakage assay of cell death in (A). Data represents the mean ± SD from 8 replications. Different letters above each bar represent a significant difference at P<0.001 using a two-way ANOVA with Dunn's test. **(C)** Results of RT–qPCR to demonstrate the silencing efficiency of RNAi constructs targeting silencing factors (SFs). Transcript levels of each gene were calculated relative to the RNAi-EV control. Bars represent the mean ± SD from three independent replicates. Three asterisks denotes a statistical difference at P<0.001 using a two-way ANOVA with Tukey's test. **(D)** Transcript levels of *RB_CDS* and *RB_IR* mRNAs following agroinfiltration of RNAi-hairpin constructs for 1 day and inoculation with *P. infestans* zoospores. RNA was extracted 2 days after pathogen inoculation. RT-qPCR analysis was performed using isoform-specific primers to measure the transcript levels of the two isoforms. Bars represent the mean ± SD from three independent replicates. **(E)** Transcript levels of *RB_CDS* and *RB_IR* mRNAs in *RB* transgenic *N. benthamiana* following treatment with DMSO (control), 1 μM Pla-B, or 30 μM Pla-B and inoculation with *P. infestans* zoospores at 2 dpi by RT-qPCR. Bars represent the mean ± SD from three independent replicates.

Supplemental Figure S5. Luciferase assay to monitor *RB* intron splicing following *P.infestans* inoculation.

(A) Representative photo of a *N. benthamiana* leaf infiltrated with agrobacterium carrying (clockwise) *RB-LUC*, *LUC*, empty vector (EV) control, or *RB_CDS-LUC*. One day after agroinfiltration, the infiltrated regions were treated with *P. infestans* or water (mock). The LUC activity was detected at 1 dpi. **(B)** The graph on the right shows results of 30 individual leaf discs isolated from leaves agroinfiltrated with each indicated construct followed by treatment with *P. infestans* or water. LUC activity measurement data represents the mean ± SD from 30 individual leaf discs from 3 experimental replicates. Relative *LUC* activity was normalized to the activity of the *35S::LUC* construct with mock treatment. ns = no significant difference and three asterisks denotes a statistical difference at P<0.001 using a two-way ANOVA with Tukey's test.

Supplemental Figure S6. *RB* intron splicing and *RB*-mediated hypersensitive response is specific to expression of IPI-O1 but not other SREs.

On the left, transcript levels of *RB_IR* and *RB_CDS* were determined by RT-PCR following agroinfiltration of SRE proteins into leaves of *RB* transgenic *N. benthamiana*. In the middle, data represent relative intensity of RT-PCR products normalized with internal control *NbEF1α*. Intensities of the bands were quantified by Image J software, and the relative abundances of *RB* isoforms are relative to *RB_CDS* at 0 dpi. Bars represent the mean ± SD from three independent replicates. ns = no significant difference and three asterisks denotes a statistical difference at P<0.001 using a two-way ANOVA with Tukey's test. On the right are representative photos of the cell death phenotypes of SRE expression in *RB* transgenic (Nb^{RB}) and wildtype *N. benthamiana* (*Nb*). The numbers represent incidence ratios of cell death responses.

Supplemental Figure S7. The splicing factor CWC15 is conserved in potato populations.

(A) Alignment comparing CWC15a and CWC15b in double-monoploid potato DM-1-3. **(B)** Alignment comparing several CWC15 homologs in different potato cultivars and wild species. Individual amino acids are depicted in color scheme, degree of overall amino acid conservation is shown both as line plot and sequence logo. Peptide sequences of CWC15 orthologues were extracted from published potato pan-genome (Tang et al., 2022). All selected protein sequences were aligned by R-msa packages (Version 1.33.0) in ClustalW method, and visualized by Jalview (Verion 2.11.0). All the CWC15 sequences used in the analysis were listed in the Data Set S3.

Supplemental Figure S8. IPI-O1 interacts with StCWC15a/b, but IPI-O1^{nls} cannot.

IPI-O1 interacts with StCWC15 in the nucleolus and nuclear speckles. Split-YFP/BiFC of IPI-O1 or IPI-O1^{nls} and Pi04314 with StCWC15a and b using fluorescence imaging. Samples were stained with 2 ug/mL DAPI to indicate the nucleus. Numbers represent the frequency of cells showing YFP fluorescence compared to the total number of cells in the 25mm^2 discs from three biological replicates. Bar = 5 μm.

Supplemental Figure S9. StCWC15 is localized in the nucleoplasm.

(A) StCWC15a/b-RFP were expressed in *N. benthamiana* leaves for 48 h before imaging. Numbers represent the frequency of subcellular localization in indicated cellular structure compared to the total fluorescent cells in the 25mm^2 range. Bar = 5 μm. **(B)** Immunoblot analysis of protein in co-localization experiment. RFP tag fusions with StCWC15a/b were confirmed by protein blotting using an anti-RFP antibody. Protein loading is visualized by Ponceau S staining. GFP tagged fusions with IPI-O1, IPI-O1^{nls} and GFP proteins were confirmed by protein blotting using an anti-GFP antibody.

Supplemental Figure S10. **Nuclear speckle accumulation of StCWC15 is mediated by *P. infestans* during infection.**

(A) Images are representative of the different patterns observed in GFP–StCWC15 re-localization from the nucleoplasm to speckles. Nucleolar GFP–StCWC15 fluorescence near the haustoriated cells detected in speckles (upper panel) while in cells distant from the haustoriated cells, it remained in the nucleoplasm (lower panel). Images are representative of the GFP protein localization pattern during *P. infestans* infection. Bar =5 μm. **(B)** Data represents the number of CWC15-positive speckles during *P. infestans* infection. Bars represent the mean ± SD of 10 replications from three independent replicates. ns = no significant difference and three asterisks denotes a statistical difference at P<0.001 using a one-way ANOVA with Tukey's test.

Supplemental Figure S11. **Splicing factor CWC15 is specifically involved in *RB*-mediated hypersensitive response.**

(A) Silencing of *CWC15* leads to loss of *RB*-mediated HR. IPI-O1 was co-expressed with the indicated RNAi constructs in *RB* transgenic *N. benthamiana*. Numbers represent the incidence ratios of hypersensitive cell death responses. Infiltrated areas were photographed 4 dpi. Electrolyte leakage was monitored by conductivity measurements following the same treatments (bottom). Data represents the mean ± SD from 12 replications. Different letters designate a significant difference from the empty vector (EV) control at P<0.001. **(B)** The

designated Avr/R gene combinations were co-agroinfiltrated in *N. benthamiana* leaves following silencing of *CWC15*. The HR phenotype was photographed at 4 dpi. The numbers represent incidence ratios of cell death responses (upper). Below shows the results of electrolyte leakage assays of infiltrated areas. Data represents the mean ± SD from 12 replications. ns = no significant difference and three asterisks denotes a statistical difference at P<0.001 using two-way ANOVA with Tukey's test.

Supplemental Figure S12. *CWC15* silencing in *N. benthamiana* by VIGS showed deficiency in growth and immunity.

(A) Schematic diagram showing the fragments used in VIGS constructs. **(B)** The morphology of *NbCWC15* silencing in *N. benthamiana*. Two-week-old *N. benthamiana* plants were infiltrated with agrobacterium carrying TRV: EV, TRV: 5'*NbCWC15*, TRV: 3'*NbCWC15* and TRV: *PDS*, respectively. The photo was taken 3 weeks after infiltration. Bar = 3 cm. **(C, D)** HR induced by IPI-O1 and RB was impaired in *NbCWC15* silenced *N. benthamiana*. (C) 3' *NbCWC15* or 5' *NbCWC15* silencing has disturbed the recognition of IPI-O1 by RB. Hypersensitive cell death phenotypes were photographed at 4 dpi. The numbers represent incidence ratios of hypersensitive cell death responses. **(D)** Electrolyte leakage from the infiltrated leaf discs was measured as a percentage of leakage from boiled discs at 4 dpi. Data represents the mean ± SD from 10 replications. Three asterisks denote a statistical difference at P<0.001 using a one-way ANOVA with Tukey's test. **(E)** Silencing efficiency of *NbCWC15* in *N. benthamiana*. Bars represent mean ± SD of three independent replicates. Two asterisks denote a statistical difference at P<0.05 using two-way ANOVA with Tukey's test.

Supplemental Figure S13. *CWC15* silencing has no effect on *RB_CDS* recognition of IPI-O1.

(A) *CWC15* silencing impairs RB/IPI-O1 induced HR and not RB_CDS/IPI-O1, R3a/Avr3a, or INF1. R gene/effector combinations and INF1 were agroinfiltrated into *NbCWC15*-silenced *N. benthmiana* leaves. Photos of HR phenotypes were taken at 4 dpi. The numbers represent incidence ratios of hypersenisitve cell death responses. **(B)** Quantification

of cell death by measuring electrolyte leakage at 4 dpi. Bars represent the mean ± SD from 12 replications. ns=no significant difference and three asterisks denotes a statistical difference at P<0.001 using a two-way ANOVA with Tukey's test.

Supplemental Figure S14 StCWC15 synthetic sequences complement *CWC15* silencing causing *RB*-mediated immunity deficient.

(A) Schematic representation of VIGS and complementation design. The region from 460~696bp of *NbCWC15* was cloned into VIGS construct TRV2-3'*NbCWC15* for silencing. Synonymous substitutions were introduced into the synthetic StCWC15 ($StCWC15^{syn}$) without changing the protein sequence. The nucleotide and protein sequence alignments indicate the synonymous changes in the synthetic variant. **(B)** Expression of silencing-resistant synthetic StCWC15 ($StCWC15a^{syn}$/ $StCWC15b^{syn}$) rescues *RB*–mediated HR in *NbCWC15*-silenced *N. benthamiana* plants. GFP and StCWC15a and StCWC15b were used as controls. Below shows results of electrolyte leakage assays of infiltrated areas at 4 dpi. The number represents incidence ratios of cell death responses. Bars represent the mean ± SD from 12 replications. Three asterisks denotes a statistical difference from the control at P<0.001 using a two-way ANOVA with Tukey's test. **(C-D)** Immunoblot analysis of StCWC15a/b, $StCWC15a^{syn}$/$StCWC15b^{syn}$ in EV (C) and *CWC15*-silenced (D) plants. C-terminal GFP-tagged StCWC15 variants were transiently expressed in VIGS control and *CWC15*-silenced *N. benthamiana*. Protein loading is visualized by Ponceau S staining.

Supplemental Figure S15. *RB_CDS* transgenic plant exhibit slowed growth.

(A) Photos of cv. Favorita expressing wildtype *RB* ($Favorita^{RB}$) or *RB_CDS* ($Favorita^{RB_CDS}$) from initial transplanting (0d) to 75 days after transplanting. Bar = 3cm. **(B)** The height of the transgenic plants graphed over time. Data points combine measurements from 5 individual transgenic plants. Data represent the mean ± SD from 3 replicates. Statistical differences among the samples were analyzed with a one-way ANOVA with Dunn's test (P<0.001).

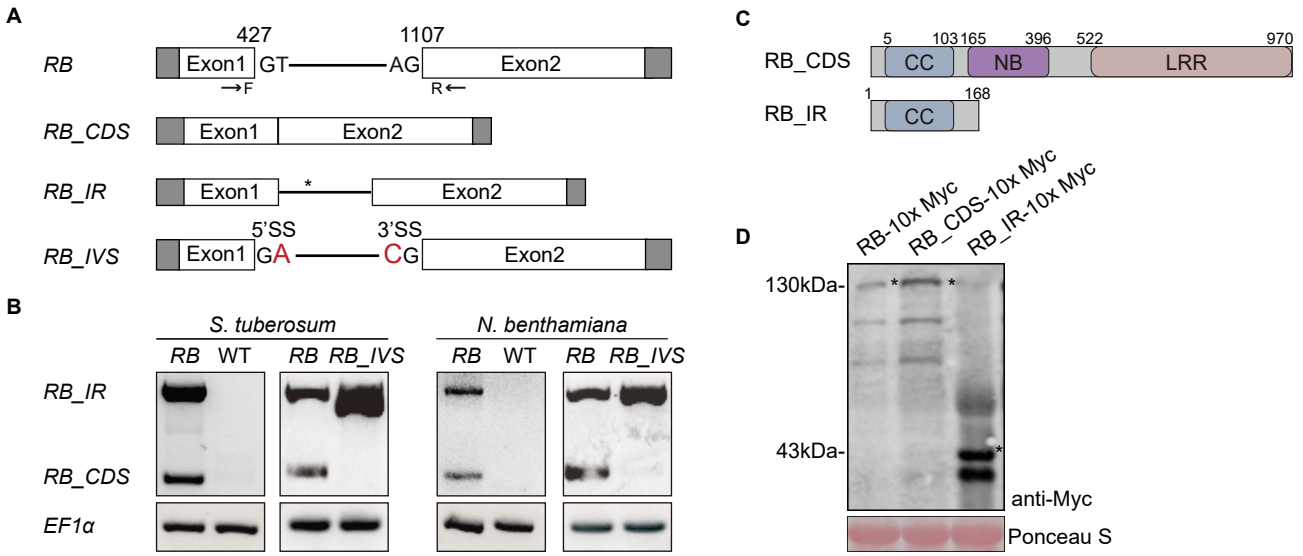

Figure 1. The *RB* intron is alternatively spliced.

(A) Gene model and splicing isoforms of *RB*. 5' and 3' UTRs are shaded grey. The intron is denoted by a black line. The asterisk shows the location of a premature termination codon. The arrows indicate the primers used in (B). Red letters in *RB_IVS* denote mutations to change the intron splicing recognition sites. **(B)** RT-PCR of *RB* and *RB_IVS* splicing mutant from transgenic *S. tuberosum* cv. Favorita and transgenic *N. benthamiana*. *RB_IR* is 995bp, and *RB_CDS* is 316bp. cDNA of Favorita and wildtype *N. benthamiana* were used as negative controls. *StEF1α* and *NbEF1α* were used as internal controls. **(C)** Diagrams showing the domains present in each of the predicted proteins produced from transcripts. **(D)** Expression of Myc-tagged fusions of *RB*, *RB_CDS*, and *RB_IR* in *N. benthamiana* was confirmed by western blotting using an anti-Myc antibody. The asterisk stands for the predicted protein RB RB_CDS and RB_IR. Equal protein loading was visualized by Ponceau S staining.

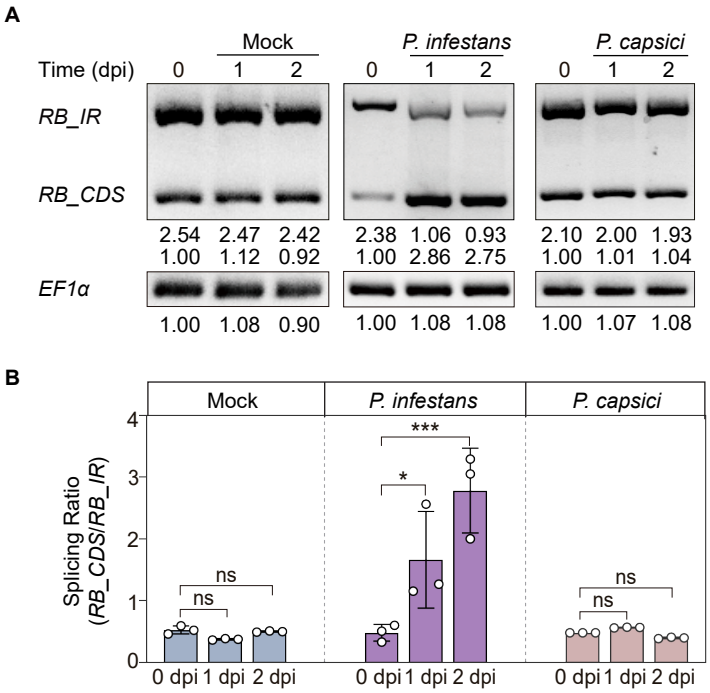

Figure 2. *RB* intron splicing is specifically induced following *P. infestans* inoculation.
(A) RT-PCR of variants *RB_IR* or *RB_CDS* in *RB* transgenic potato following inoculation with water (mock), *P. infestans* JH19 or *P. capsici* LT1534. *StEF1α* was used as the internal control. **(B)** Splicing ratio of *RB* in transgenic potato following inoculation with water (mock), *P. infestans* JH19, or *P. capsici* LT1534. Transcript levels were detected by RT-qPCR and normalized to *RB_CDS* following mock treatment at 0 dpi. Bars represent the mean ± SD from three independent replicates. ns = no significant difference, one asterisk denotes a significant difference at P<0.05, and three asterisks denotes a significant difference at P<0.001 using a two-way ANOVA with Tukey's test.

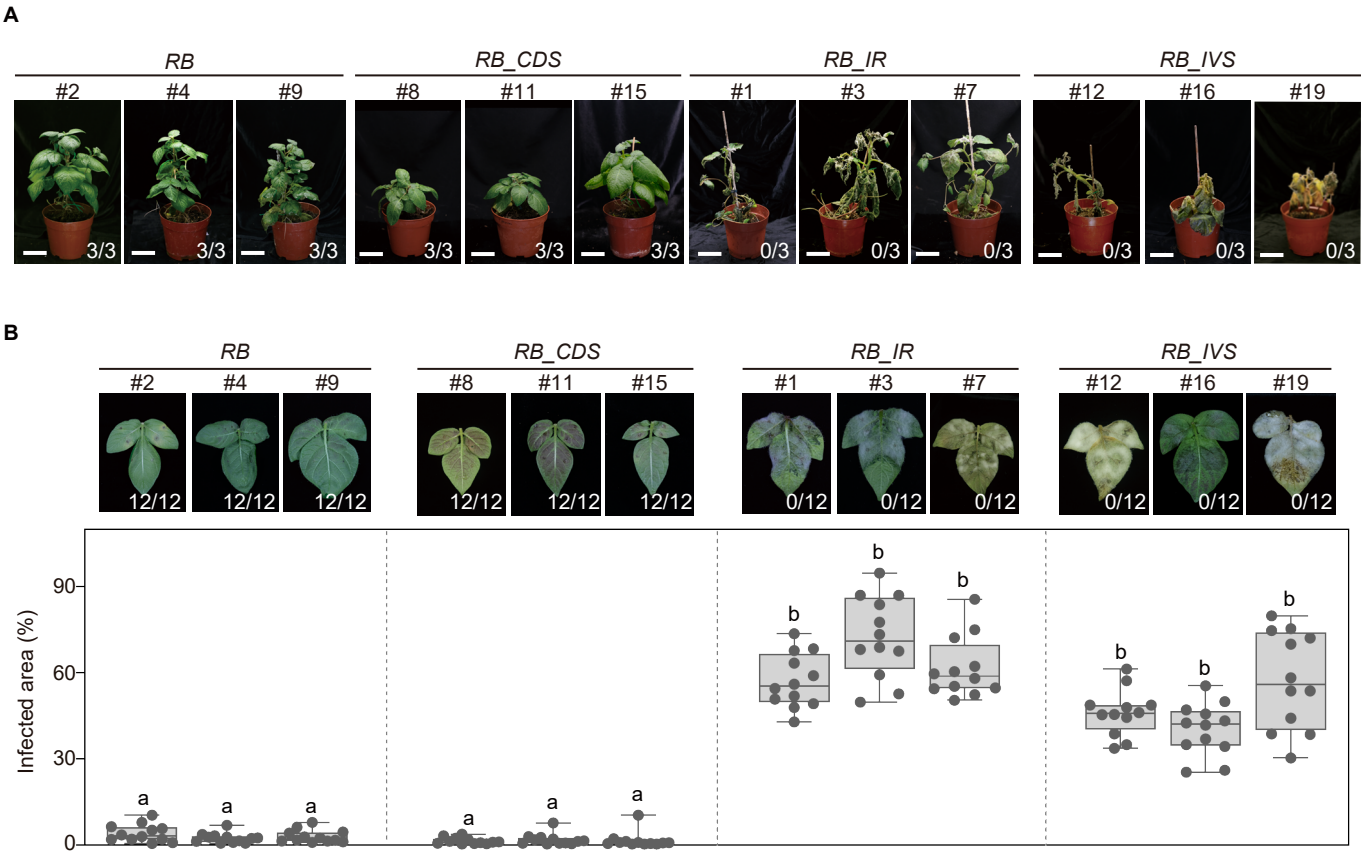

Figure 3. Intron retention in *RB* results in susceptibility to *P. infestans.*
(A) Zoospore suspension of *P. infestans* strain JH19 was used to inoculate *RB*, *RB_CDS*, *RB_IR* and RB^{IVS} transgenic potato plants at a concentration of 15,000 zoospores/ml . Plants were photographed at 5 dpi. The numbers represent the ratio of resistant plants compared to all inoculated plants. Bar = 5 cm. **(B)** Zoospore suspension of *P. infestans* strain JH19 was drop-inoculated on detached leaves of *RB* transgenic potato expressing the indicated gene variants. The infected leaves were photographed at 4 dpi. The numbers represent the ratio of resistant leaves compared to all inoculated leaves. Bars represent the percent infected area of the detached leaves. The data represents the mean ± SD from 12 replications. Different letters above bars denote a significant difference at P<0.001 using a two-way ANOVA with Dunn's test..

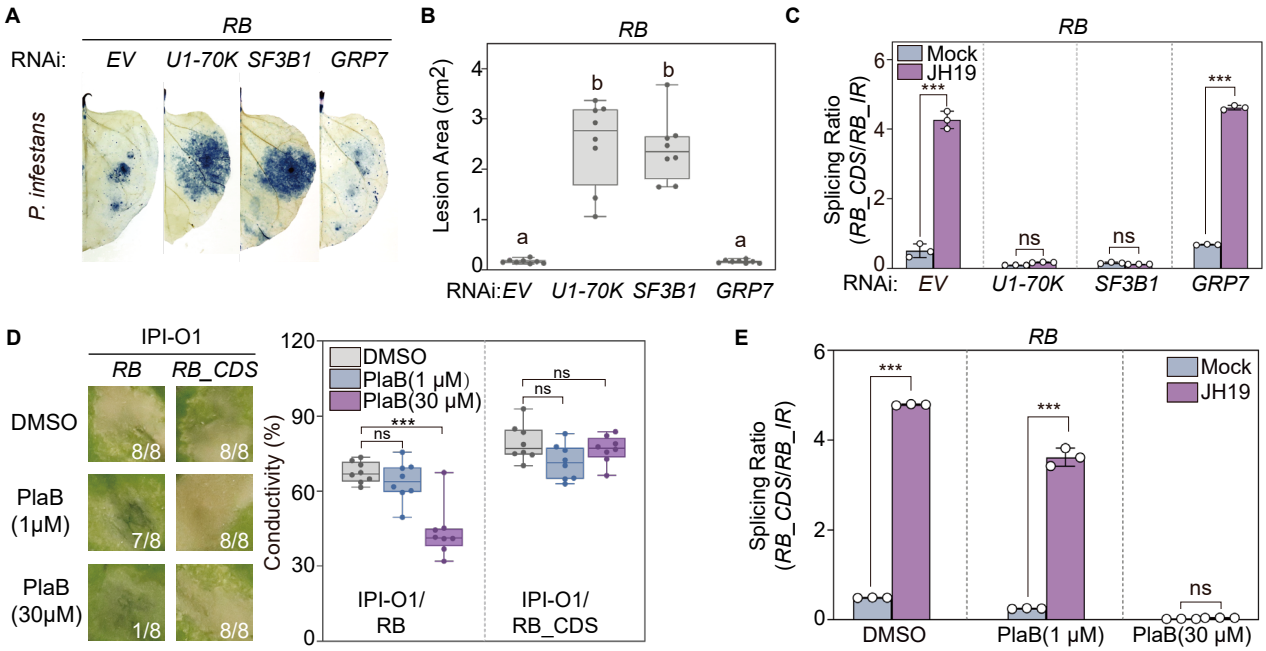

Figure 4. Spliceosome activity is necessary for *RB*-mediated resistance to *P. infestans*.
(A) Trypan blue staining of *RB* transgenic *N. benthamiana* following agroinfiltration of RNAi-hairpin constructs and inoculation with *P. infestans* zoospores. EV = empty vector control. Leaves were photographed at 5 dpi. **(B)** Lesion areas (cm^2) of inoculated leaves in (A). Data represents the mean ± SD from 8 replicates. Different letters above bars denotes a significant difference at P<0.001 using a one-way ANOVA with Dunn's test. **(C)** Splicing ratio of *RB* in *RB* transgenic *N. benthamiana*following agroinfiltration of RNAi-hairpin constructs for 1 day and inoculation with *P. infestans* zoospores. RNA was extracted 2 days after pathogen inoculation. Transcript levels were detected by RT-qPCR and normalized to RB_CDS in RNAi-EV and following mock treatment. Bars represent the mean ± SD in three independent replicates. **(D)** Agroinfiltration of IPI-O1 in *RB* and *RB_CDS* transgenic *N. benthamiana* with DMSO (control), 1μM splicing modulator Pladienolide B (Pla-B), or 30μM Pla-B. Cell death was visually assessed and photographed at 4 dpi (left). Numbers show the ratio of infiltrated areas with cell death compared to the areas showing no cell death. Electrolyte leakage was monitored by conductivity measurements following the same treatments (right). Data represents the mean ± SD from 8 replications. **(E)** Splicing ratio of *RB* in *RB* transgenic *N. benthamiana* following treatment with DMSO (control), 1μM Pla-B, or 30μM Pla-B and inoculation with *P. infestans* zoospores at 2 dpi by RT-qPCR. For all graphs, ns = no significant difference and three asterisks denotes a statistical difference at P<0.001 using a two-way ANOVA with Tukey's test..

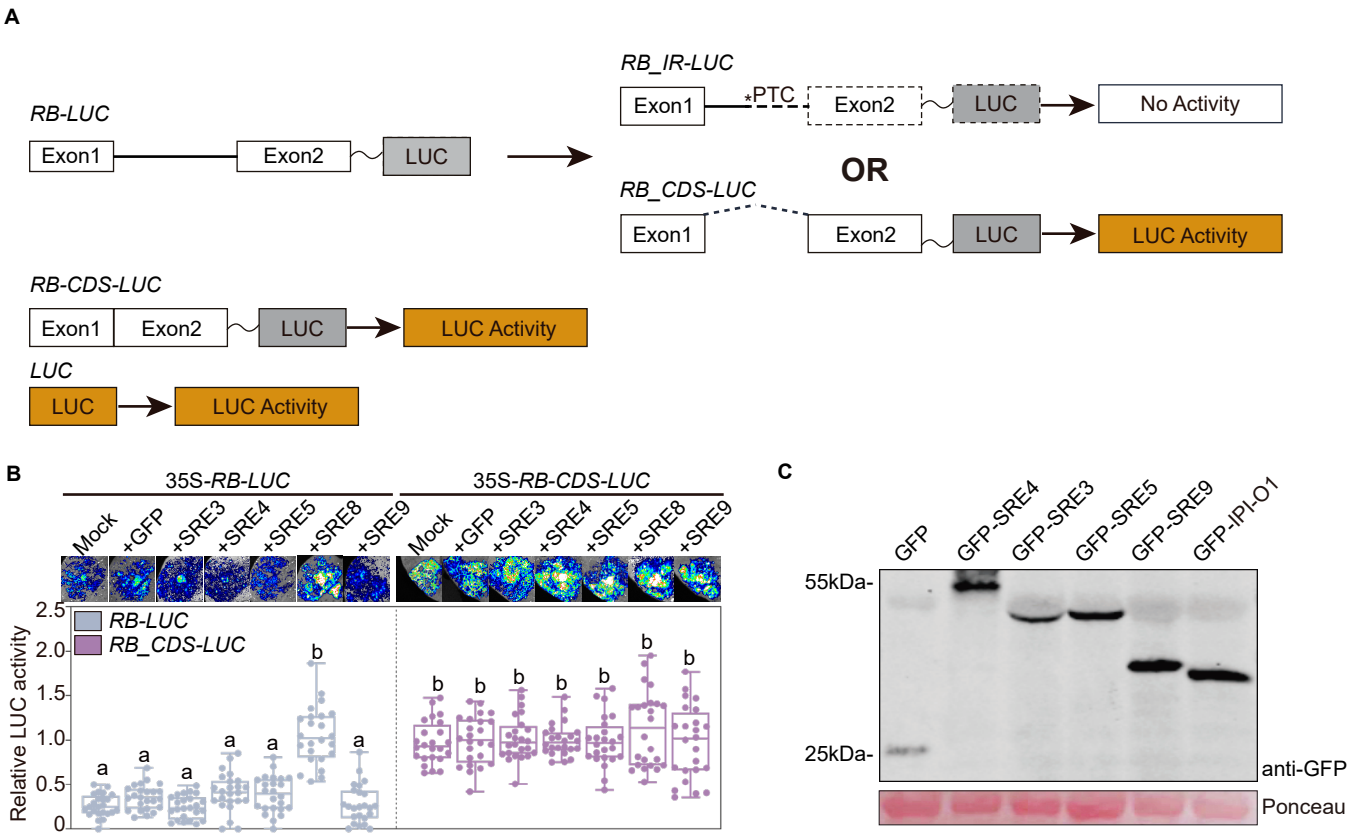

Figure 5. IPI-O1 induces *RB* intron splicing.
(A) Schematic diagram of the *RB_LUC* alternative splicing reporter system. The genomic sequence of *RB* was fused with the *luciferase* (*LUC*) gene to construct 35S::*RB-LUC*. Intron retention introduces a premature termination codon (PTC) and no production of the luciferase reporter. Intron splicing leads to a full-length RB-LUC protein with luciferase activity. The 35S::*RB_CDS-LUC* construct with the intron removed produces a full-length RB-LUC protein with luciferase activity regardless of intron splicing activity. The 35S::*LUC* construct is a positive control. **(B)** Results of co-expression of the reporters with multiple splicing regulatory effectors (SRE; Huang et al., 2020). LUC activity was quantified at 48 hpi. 24 individual leaf discs were collected for LUC activity measurement, and relative LUC activity was normalized to the activity of the 35S::*RB_CDS-LUC* construct with mock treatment. Data represents the mean ± SD from 24 replications. Different letters above each bar represent a significant difference at P<0.001 using a two-way ANOVA with Dunn's test. **(C)** GFP-tagged SRE fusion protein expression in *N. benthamiana* was confirmed by western blotting using an anti-GFP antibody. Protein loading was visualized by Ponceau S staining.

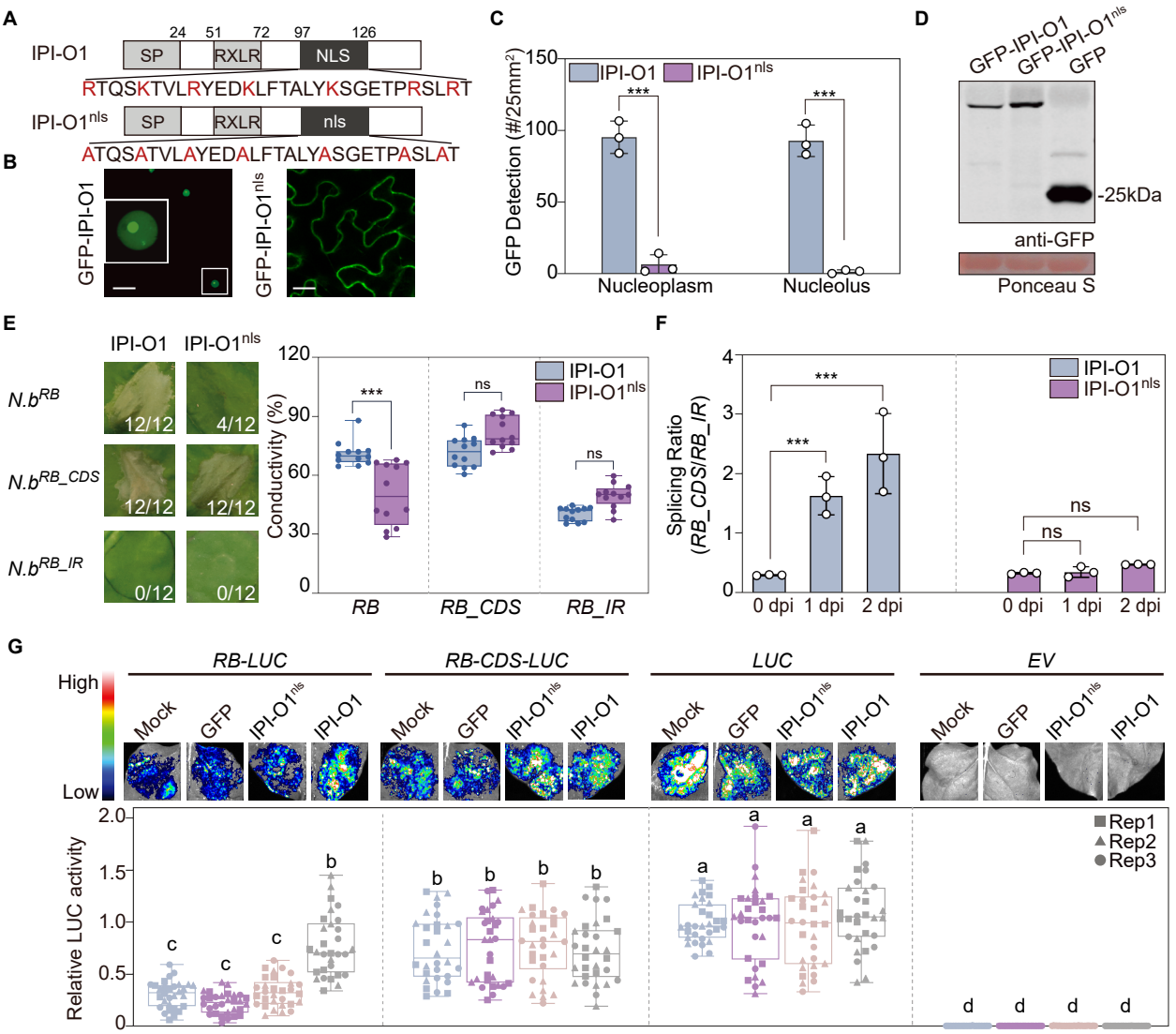

Figure 6. Nuclear localization of IPI-O1 is necessary for *RB* intron splicing.
(A) Schematic diagrams at the top show the location of alanine replacements within the nuclear localization signal of IPI-O1. GFP-IPI-O1 and GFP-IPI-O1^{nls} were expressed in *N. benthamiana* leaves for 48 h before imaging, Scale bar = 20 µm. **(B)** Bars represent the number of times that GFP was detected in the nucleoplasm or nucleolus following infiltration of GFP-IPI-O1 and GFP-IPI-O1^{nls}. Data represents the mean ± SD of three replicates. **(C)** Expression of GFP-tagged fusions of IPI-O1 and IPI-O1^{nls} in *N. benthamiana* was confirmed by western blotting using an anti-GFP antibody. Protein loading was visualized by Ponceau S staining. **(D)** On the left are visual examples and incidence ratios of hypersensitive cell death responses following agroinfiltration of IPI-O1 and IPI-O1^{nls} in leaves of *RB*, *RB_CDS*, and *RB_IR* transgenic *N. benthamiana*. Cell death was visually assessed and photographed at 4 dpi. The right shows results of electrolyte leakage assays of infiltrated areas. Data represents the mean ± SD of 12 replications. **(E)** Splicing ratio of *RB* in *RB* transgenic *N. benthamiana* following agroinfiltration of IPI-O1 and IPI-O1^{nls} at 2 dpi by RT-qPCR. Bars represent the mean ± SD of three independent replicates. **(F)** Results of co-expression of *RB LUC* reporters with mock, GFP, IPI-O1 and IPI-O1^{nls} in *N. benthamiana* leaves by agroinfiltration. LUC activity was quantified at 2 dpi. Relative LUC activity was normalized to the activity of the 35S-LUC construct with mock treatment. Data represents the mean ± SD of 30 replications. For all graphs, ns = no significant difference and three asterisks denotes a statistical difference at P<0.001 using a two-way ANOVA with Tukey's test..

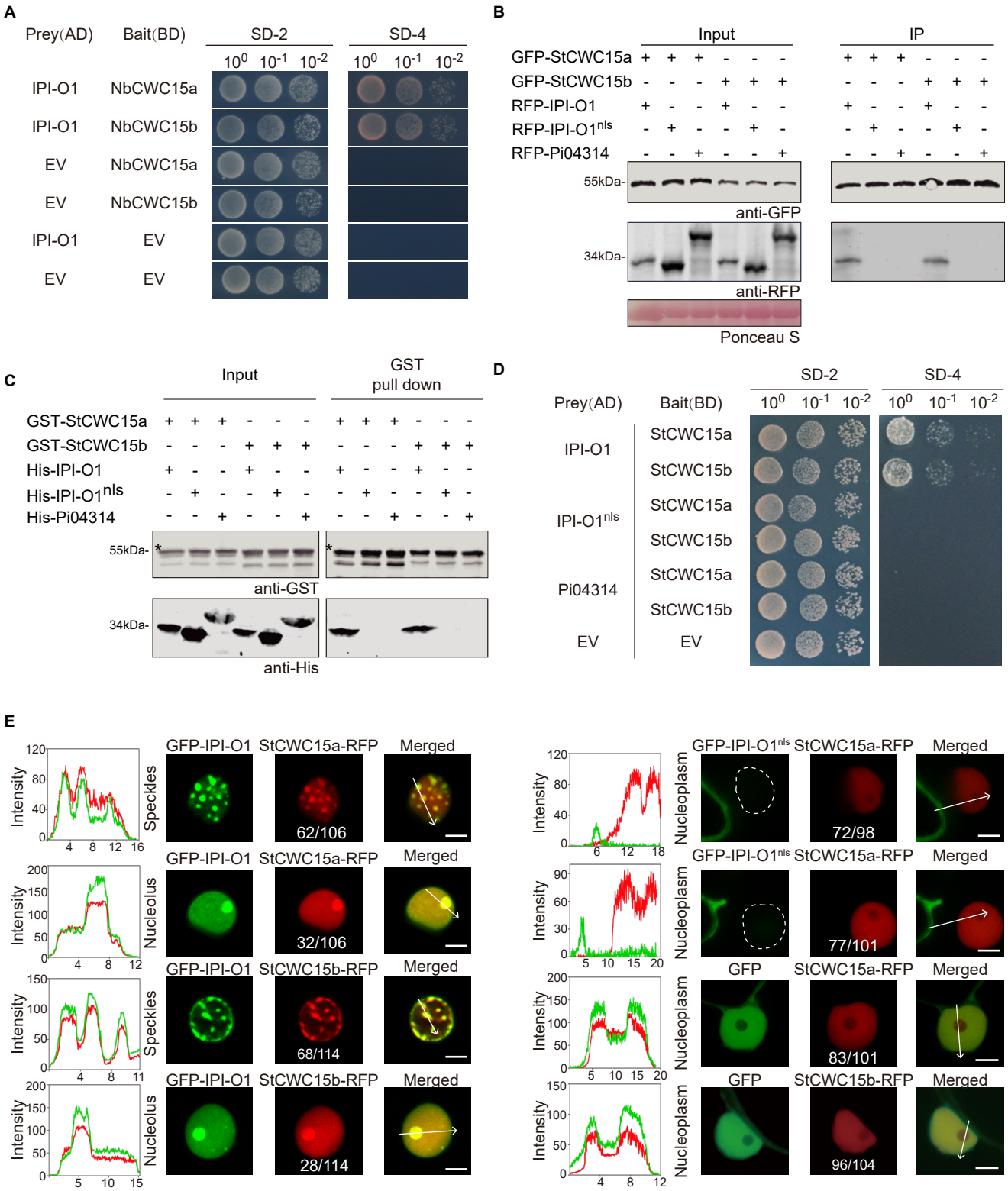

Figure 7. IPI-O1 interacts physically with splicing factor CWC15.
(A) Yeast-two hybrid interaction between IPI-O1, CWC15 variants, and splicing factors from *N. benthamiana*. Yeast transformants were spotted as 10-fold serial dilutions on SD medium without leucine and tryptophan (SD–2), or without histidine, leucine, adenine, and tryptophan (SD–4). Yeast cells were photographed 2-3 days after plating. Empty BD and AD plasmids (EV) were used ascontrols. Experiments were performed at least three times with similar results. **(B)** Silencing of *CWC15* leads to loss of *RB*-mediated HR. IPI-O1 was co-expressed with the indicated RNAi constructs in *RB* transgenic *N. benthamiana*. Numbers represent the incidence ratios of hypersensitive cell death responses. Infiltrated areas were photographed 4 dpi. Electrolyte leakage was monitored by conductivity measurements following the same treatments (bottom). Data represents the mean ± SD from 12 replications. Different letters designate a significant difference from the empty vector (EV) control at $P<0.01$.
(C) Immunoprecipitation (IP) of StCWC15a/b-GFP with RFP-IPI-O1, RFP-IPI-O1^{nls}, or RFP-Pi04314 following agroinfiltration in *N. benthamiana* leaves. Expression of constructs in the leaves is indicated by +. Protein size markers are indicated in kDa, and the Ponceau S stain was used to show levels of protein loading. **(D)** *In vitro* pulldown assay using the GST-tagged StCWC15a/b to immunoprecipitate IPI-O1 and IPI-O1^{nls}. Input

and GST-pulldown proteins were visualized by protein blotting using anti-GST and anti-His antibodies. Asterisks (*) indicate the protein bands that correspond to the expected size of CWC15. **(E)** IPI-O1 co-localizes with StCWC15 in nuclear speckles and the nucleolus. GFP-IPI-O1, GFP-IPI-O1^{nls}, and GFP alone were transiently co-expressed with StCWC15a/b-RFP by agroinfiltration in *N. benthamiana*. The left image is from the GFP channel, the middle image is from the RFP channel, and the right image is the overlay of the GFP and RFP channels. Numbers represent the frequency of cells showing indicated StCWC15 subcellular localization compared to the total StCWC15-positive cells in 25mm^2 discs from three biological replicates. Graphs show the fluorescence intensity profiles across the arrows in the merged images. Bar = 5μm.

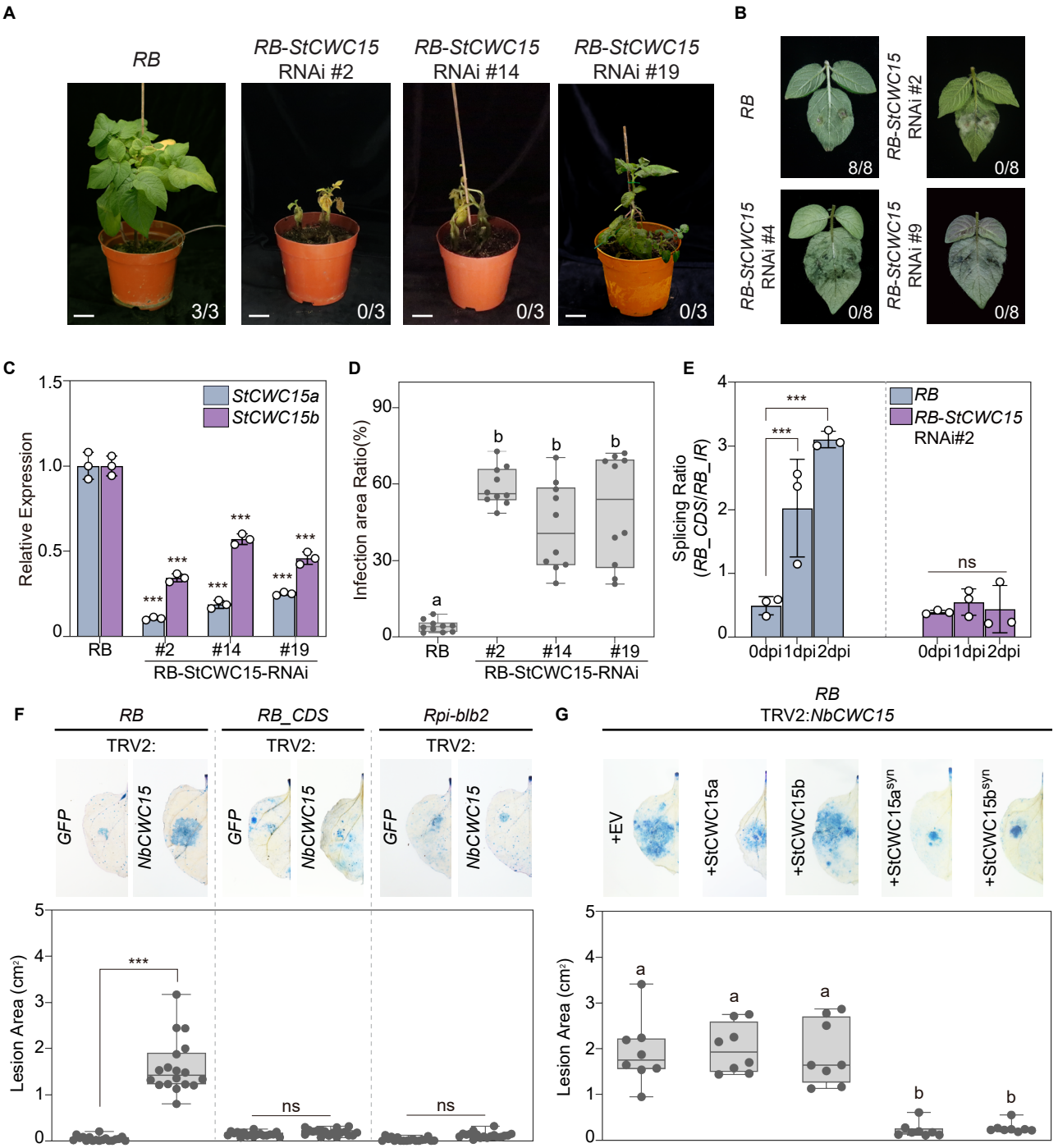

Figure 8. Silencing *StCWC15* disrupts *RB*-mediated resistance.
(A) Whole plants were spray-inoculated (left) and detached leaves were drop-inoculated (right) with zoospores of *P. infestans* strain JH19 in *RB* and *RB-StCWC15* RNAi transgenic potato. Bar = 3 cm. The number represents the frequency of leaves showing resistance compared to all inoculated leaves. **(B)** Relative expression of *StCWC15a/b* in three RNAi transformed lines compared to *RB* transgenic potato. Bars represent the mean ± SD of three independent replicates. Three asterisks designate a statistical difference from the RB control at P<0.01. **(C)** Infection ratio of *P. infestans* JH19 on *RB* and *RB-StCWC15* RNAi transgenic potato lines. Data represents the mean ± SD from 10 repliactions. Different letters denote a significance difference at P<0.001. **(D)** Splicing ratio of *RB* in *RB-StCWC15* RNAi transgenic potato line #2 following inoculation with *P. infestans* zoospores at 2 dpi by RT-qPCR. Bars represent the mean ± SD from three independent replicates. ns=no significant difference and three asterisks denotes a statistical difference at P<0.001. **(F)** *NbCWC15* was silenced by VIGS in *RB*, *RB_CDS*, and *Rpi_blb2* transgenic *N. benthamiana* and inoculated with *P. infestans* JH19 on detached leaves. Photos (top) and lesion areas (bottom) were recorded at 5 dpi. Lesion area data represents the mean ± SD from 18 replications. **(G)** Complementation of *RB* function caused by *CWC15* silencing in *N. benthamiana* via synthetic *StCWC15* constructs (*StCWC15a/b*^{syn}). Agrobacterium expressing *StCWC15a/b*^{syn} constructs were infiltrated into *NbCWC15* silenced *RB* transgenic *N. benthmiana*, then inoculated with *P. infestans* JH19 zoospores. Photos and lesion areas were recorded at 5 dpi. Data represent the mean ± SD from 8 replications. Different letters denote a significance difference at P<0.001 using one-way ANOVA with Dunn's test.

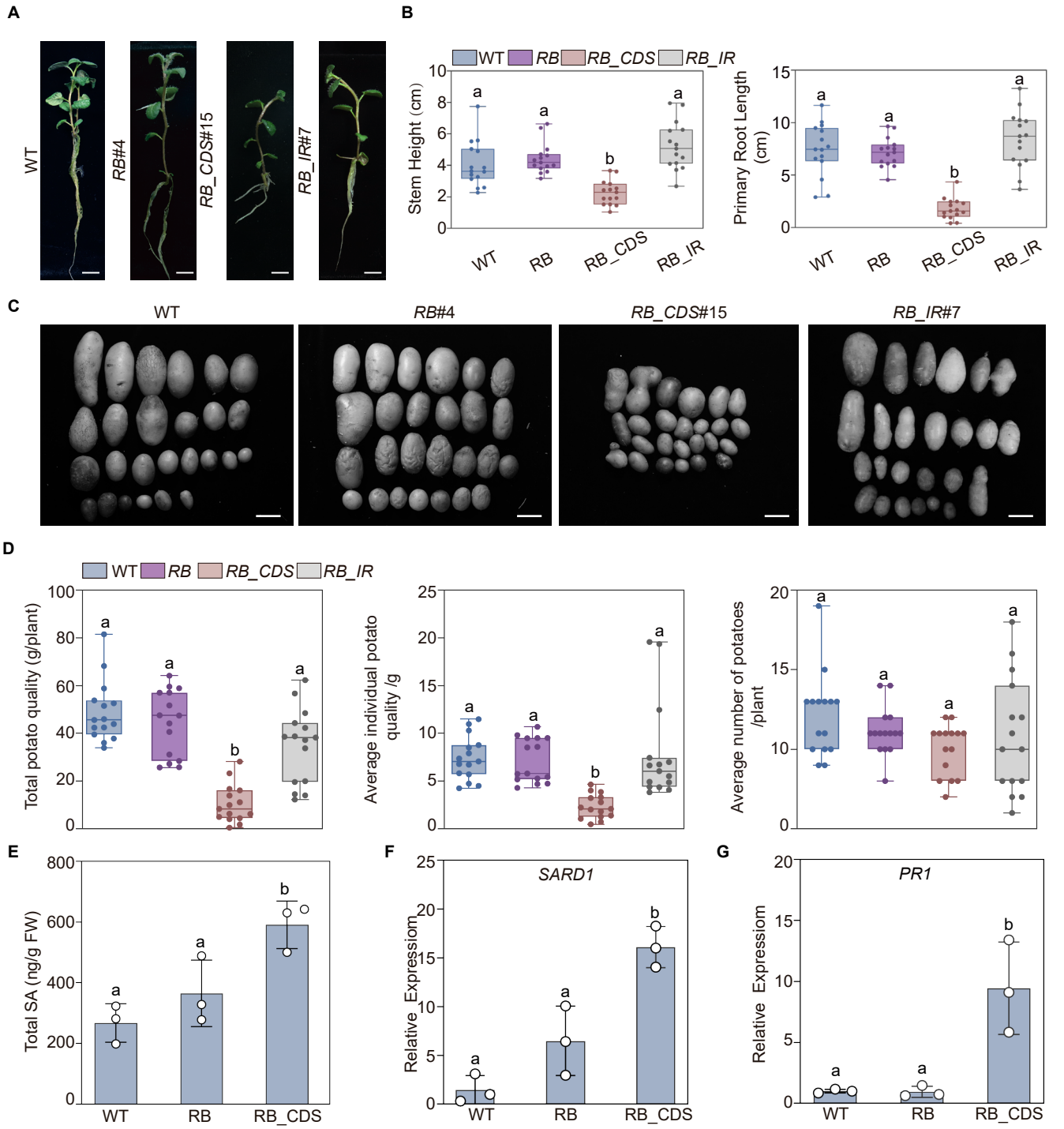

Figure 9. Alternative intron splicing of *RB* balances plant growth and immunity.
(A) Photos of 21-day-old wild-type (WT) Favorita and *RB*, *RB_CDS*, and *RB_IR* transgenic tissue culture plants. Bar = 1 cm. **(B)** Average stem height and root length of Favorita (WT) and 21 day-old transgenic potato tissue culture plants. Bars represent the mean ± SD from 15 tissue culture plants. **(C)** Tubers of Favorita (WT) and transgenic plants. Tubers were harvested and photographed 8 to 10 weeks after tissue culture plants were transplanted. Bar = 1 cm. **(D)** Average tuber yield, average individual tuber mass, and average number of tubers from greenhouse grown plants. Measurements were taken at 8 to 10 weeks after tissue culture plants were transplanted. Bars represent the mean ± SD from 15 replications of 3 independent lines for each genotype. **(E)** Total salicylic acid (SA) content in Favorita (WT) and transgenic *RB* and *RB_CDS* lines without pathogen inoculation. FW, fresh weight. Bars represent the mean ± SD from three independent replicates. **(F-G)** Relative expression of *SARD1* (F) and *PR1* (G) in the indicated transgenic potato as determined by RT-qPCR. Bars represent the mean ± SD from three independent replicates. For all graphs, different letters represent a statistical difference at P<0.001 using one-way ANOVA with Dunn's test.

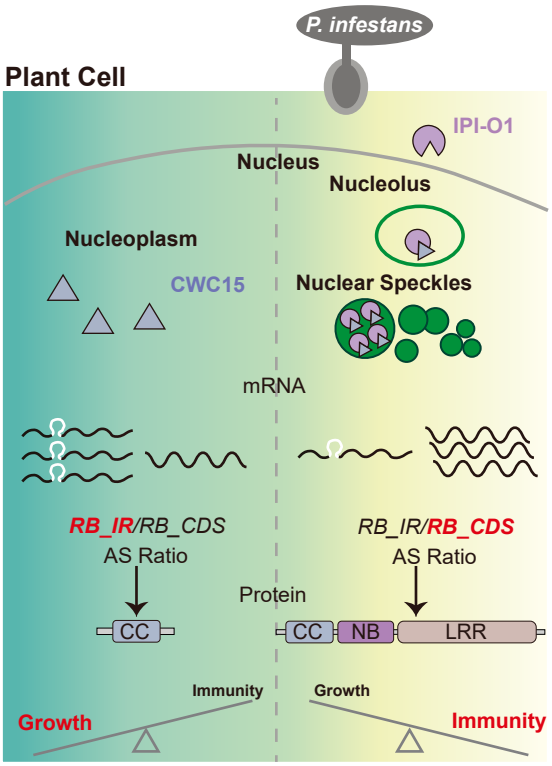

Fig.10 Schematic model of the *P. infestans*-host pathosystem related to resistance gene *RB* and effector IPI-O1.
During normal growth (left), CWC15 proteins (grey triangles) are maintained in the nucleoplasm and *RB* transcripts exist primarily with the intron retained (*RB_IR*). This results in the production of a truncated, non-functional RB protein that supports growth over immunity. Following *P. infestans* infection, effector IPI-O1 is introduced into the plant cell and translocates to the nucleus, leading to a re-localization of CWC15 from the nucleoplasm to the nucleolus and speckles. This results in increased splicing of the RB intron (*RB_CDS)*, resulting in production of a full-length RB protein that can elicit immunity.